Neurobiology of Disease 143 (2020) 105018

Contents lists available at ScienceDirect

Neurobiology of Disease

journal homepage: www.elsevier.com/locate/ynbdi

Disruption of the sodium-dependent citrate transporter SLC13A5 in mice causes alterations in brain citrate levels and neuronal network excitability in the hippocampus

Christine Henke[a,b,1], Kathrin Töllner[c,1], R. Maarten van Dijk[d], Nina Miljanovic[d], Thekla Cordes[e], Friederike Twele[c], Sonja Bröer[c], Vanessa Ziesak[f], Marco Rohde[f], Stefanie M. Hauck[g], Charlotte Vogel[h], Lisa Welzel[c,i], Tina Schumann[a,b], Diana M. Willmes[a,b], Anica Kurzbach[a,b], Nermeen N. El-Agroudy[a,b], Stefan R. Bornstein[a], Susanne A. Schneider[j], Jens Jordan[k], Heidrun Potschka[d], Christian M. Metallo[e,l], Rüdiger Köhling[f], Andreas L. Birkenfeld[a,b,2], Wolfgang Löscher[c,i,*,2]

[a] Section of Metabolic and Vascular Medicine, Medical Clinic III, Dresden University School of Medicine, Technische Universität Dresden, Germany
[b] Paul Langerhans Institute Dresden of the Helmholtz Center Munich at University Hospital and Faculty of Medicine, TU Dresden, Dresden, Germany
[c] Department of Pharmacology, Toxicology, and Pharmacy, University of Veterinary Medicine Hannover, 30559 Hannover, Germany
[d] Institute of Pharmacology, Toxicology, and Pharmacy, Ludwig-Maximilians-University, Munich, Germany
[e] Department of Bioengineering, University of California, San Diego, La Jolla, CA 92093, USA
[f] Oscar-Langendorff-Institute of Physiology, Rostock University Medical Center, Rostock, Germany
[g] Research Unit Protein Science, Helmholtz Center Munich, Neuherberg, Germany
[h] Department of Biometry, Epidemiology and Information Processing, University of Veterinary Medicine Hannover, Germany
[i] Center for Systems Neuroscience, 30559 Hannover, Germany
[j] Department of Neurology, Ludwig-Maximilians-University, Munich, Germany
[k] Institute for Aerospace Medicine, German Aerospace Center (DLR) and Chair for Aerospace Medicine, University of Cologne, Cologne, Germany
[l] Moores Cancer Center, University of California, San Diego, La Jolla, CA 92037, USA

ARTICLE INFO

Keywords:
Epilepsy, NaCT
Proteom
Metabolom
Parahippocampal cortex

ABSTRACT

In addition to tissues such as liver, the plasma membrane sodium-dependent citrate transporter, NaCT (SLC13A5), is highly expressed in brain neurons, but its function is not understood. Loss-of-function mutations in the human *SLC13A5* gene have been associated with severe neonatal encephalopathy and pharmacoresistant seizures. The molecular mechanisms of these neurological alterations are not clear. We performed a detailed examination of a *Slc13a5* deletion mouse model including video-EEG monitoring, behavioral tests, and electrophysiologic, proteomic, and metabolomic analyses of brain and cerebrospinal fluid. The experiments revealed an increased propensity for epileptic seizures, proepileptogenic neuronal excitability changes in the hippocampus, and significant citrate alterations in the CSF and brain tissue of *Slc13a5* deficient mice, which may underlie the neurological abnormalities. These data demonstrate that SLC13A5 is involved in brain citrate regulation and suggest that abnormalities in this regulation can induce seizures. The present study is the first to (i) establish the *Slc13a5*-knockout mouse model as a helpful tool to study the neuronal functions of NaCT and characterize the molecular mechanisms by which functional deficiency of this citrate transporter causes epilepsy and impairs neuronal function; (ii) evaluate all hypotheses that have previously been suggested on theoretical grounds to explain the neurological phenotype of *SLC13A5* mutations; and (iii) indicate that alterations in brain citrate levels result in neuronal network excitability and increased seizure propensity.

Abbreviations: aCSF, artificial cerebrospinal fluid; CSF, cerebrospinal fluid; EEG, electroencephalogram; fEPSP, field excitatory postsynaptic potentials; GAD, glutamate decarboxylase; NaCT, sodium-dependent citrate transporter; NMDA, *N*-methyl-D-aspartate; PTZ, pentylenetetrazole; RED, recurrent epileptiform discharges; TCA, tricarboxylic acid cycle

* Corresponding author at: Department of Pharmacology, Toxicology, and Pharmacy, University of Veterinary Medicine Hannover, 30559 Hannover, Germany
E-mail address: wolfgang.loescher@tiho-hannover.de (W. Löscher).

[1] *equal contribution*
[2] *equal contribution*

https://doi.org/10.1016/j.nbd.2020.105018
Received 4 May 2020; Received in revised form 8 July 2020; Accepted 11 July 2020
Available online 16 July 2020

1. Introduction

SLC13A5, also known as the Na^+/citrate cotransporter (NaCT) and encoded by the *Slc13a5* gene in mammals, is a Na^+-coupled transporter for citrate that is expressed in the plasma membrane of cells particularly in the liver, testis, and brain (Bergeron et al., 2013; Willmes et al., 2013; Pajor, 2014). SLC13A5 mediates the uptake of tricarboxylic acid cycle (TCA) intermediates such as citrate, succinate, and α-ketoglutarate into cells across the plasma membrane. Reducing the expression of the *Slc13a5* homolog in *D. melanogaster* and *C. elegans* significantly extends life span and promotes mitochondrial biogenesis by mechanisms akin to caloric restriction (Rogina et al., 2000; Anderson and Weindruch, 2012). Therefore, the *Drosophila* gene has been named 'INDY', an acronym for 'I'm Not Dead, Yet' (Rogina et al., 2000).

In the mouse brain, SLC13A5 is expressed in neurons of the cerebral cortex, hippocampal formation, cerebellum, and olfactory bulb (Inoue et al., 2002a; Wada et al., 2006; Pajor et al., 2001). In the cerebral cortex of rats, neuronal *Slc13a5* expression is known to increase during postnatal development, reaching much higher levels in adult animals (Yodoya et al., 2006). SLC13A5 is also expressed in neurons of the human brain (Inoue et al., 2002b; Bhutia et al., 2017), however, the potential role of SLC13A5 for neuronal excitability or functionality is presently not known (Bergeron et al., 2013; Bhutia et al., 2017). In mice, but not rats, SLC13A5 has also been detected in astrocytes (Pajor, 2014).

The interest in the activity of SLC13A5 and other plasma membrane transporters of TCA cycle intermediates in the brain is driven in part by the assumption that neurons do not express pyruvate carboxylase (Cesar and Hamprecht, 1995). Therefore, neurons should not be able to synthesize TCA intermediates de novo. Further, plasma membrane transporters of TCA cycle intermediates are assumed to be important for maintaining normal metabolism (Yu et al., 1983; Shank et al., 1985; Cesar and Hamprecht, 1995). Interestingly, despite the lack of pyruvate carboxylase, normal neuronal pyruvate carboxylation rates have been described that resemble those seen in glial cells (Hassel and Brathe, 2000; Hassel, 2001). The pathway by which neurons synthesize TCA cycle intermediates is not yet understood.

Recently discovered loss-of-function mutations in the human *SLC13A5* gene have been linked to the development of early-onset epileptic encephalopathy. Affected individuals can have recurrent and pharmacoresistant seizures as early as the first day of life (Thevenon et al., 2014; Hardies et al., 2015; Klotz et al., 2016; Bainbridge et al., 2017; Schossig et al., 2017; Weeke et al., 2017; Alhakeem et al., 2018; Grinspan et al., 2018). The clinical presentation ranges from multiple daily focal or generalized convulsive seizures, to life-threatening status epilepticus to rare seizures with rather tonic-static impairment, even in patients with the same homozygous mutations; heterozygous carriers are not affected. Functional transport studies in vitro for over a dozen different mutations in *SLC13A5* showed little to no transport activity, suggesting a loss of function (Klotz et al., 2016; Selch et al., 2018). Yet, the exact molecular mechanisms by which the functional deficiency of SLC13A5 may lead to epilepsy and impairs neuronal development and function remain to be elucidated. Interestingly, there is as yet no evidence of epilepsy or encephalopathy in *Slc13a5*-knockout mice (Bhutia et al., 2017), but it is not known whether this relates to species differences in clinical consequences of the loss of function of this transporter, or to a lack of sufficiently detailed neurological analysis of the *Slc13a5*-knockout mice. Here, we performed detailed neurological, behavioral, electrophysiological, metabolomic and proteomic brain analyses in a mouse model of *Slc13a5* deficiency, including continuous video-EEG monitoring. We recorded epileptic seizures in a fraction of the *Slc13a5*-knockout mice, thus allowing to assess the role of *Slc13a5* in the development of epileptic seizures and to delineate possible molecular mechanisms.

2. Materials and methods

2.1. Animals

The *Slc13a5*$^{-/-}$ mice (knockout-mouse model of the mammalian INDY [SLC13A5] homolog, SLC13A5) were generated on a C57BL/6J background as described previously (Birkenfeld et al., 2011). The mice were bred at the Research Institutes for Experimental Medicine of the Charité Berlin and/or the experimental center of the Medical Faculty Carl Gustav Carus of the Technische Universität Dresden, Germany and shipped to the laboratories in Hannover (video-EEG monitoring, behavioral analyses, histology) and Rostock (electrophysiology). For metabolomic and proteomic analyses, brain tissue, CSF and plasma were sampled in Dresden and samples were shipped to San Diego and Munich.

Experiments were performed according to the EU council directive 2010/63/EU and the German Law on Animal Protection ("Tierschutzgesetz"). Ethical approval for the study was granted by an ethical committee (according to §15 of the Tierschutzgesetz) and the government agency (Lower Saxony State Office for Consumer Protection and Food Safety; LAVES) responsible for approval of animal experiments in Saxony (reference number: TVV5/2016) and Lower Saxony (reference number: 16/2226). All efforts were made to minimize both the suffering and the number of animals.

Slc13a5-knockout and littermate control male and female mice were housed separately in groups under controlled environmental conditions (231°C; 50–60% humidity; 12 h light/dark cycle; light on at 6:00 a.m.) with free access to standard laboratory chow and tap water. Mice were allowed to adapt to the laboratory conditions before experiments were started. Experiments started at an age of 7 weeks (video/EEG monitoring), 10–12 weeks (behavioral analyses, metabolomics, proteomics), or 14–15 weeks (electrophysiology).

For tissue, CSF and plasma sampling, mice were fasted 4 h in the morning and CSF punctuation or sacrificing was performed. All animal experiments of this study are reported in accordance with ARRIVE guidelines (Kilkenny et al., 2010).

2.2. Hippocampal electrode implantation in mice

Bipolar electrodes for the recording of electroencephalograms (EEGs) were stereotactically implanted into the right CA1 area of the dorsal hippocampus in 20 mice (5 mice each for male and female wildtype and knock out, respectively). Stereotaxic coordinates for EEG electrode implantation are shown in Table S1. In preliminary experiments in groups of 4 mice, stereotaxic coordinates (according to Paxinos and Franklin (2001) were determined for each genotype and sex by histological verification of the implantation site in the CA1. The surgery was performed under anesthesia with ketamine (70 mg/kg i.p.; Ketamin 10%, Medistar, Ascheberg, Germany) and xylazine (14 mg/kg i.p.; Rompun® 2% Bayer, Monheim, Germany). To prevent postoperative infection, mice were treated with marbofloxacin (4 mg/kg s.c., once daily; Marbocyl FD 1%, Vetoquinol, Ravensburg, Germany) for 7 days starting two days before electrode implantation.

2.3. EEG monitoring in mice

Starting one week after the surgery, 8 wildtype (*Slc13a5*$^{+/+}$) and 8 knock out (*Slc13a5*$^{-/-}$) mice were connected to a system consisting of one-channel amplifiers (Animal BioAmp FE136, ADInstruments Ltd.,

Sydney, Australia) and analogue-digital converters (PowerLab 4/35 PL3504/P, ADInstruments) for two weeks of continuous (24 h/day) EEG-monitoring. The data were recorded and analyzed with the LabChart 8 software for windows (ADInstruments; sampling rate 200 Hz; time constant 0.1 s; low pass filter 60 Hz). The EEG recording was directly linked to simultaneous digital video-recording of four mice per screen using four infrared board cameras (Sony) merged by one video quad processor (Monarcor TVSP-44COL). Mice were housed in clear plexiglass cages (one per cage) with light-colored bedding. For monitoring during the dark phase, infrared LEDs were mounted above the cages.

Every second day of the two weeks of video/EEG recordings was visually analyzed for abnormal electrographic activity, i.e. occurrence of spikes, electrographic or electroclinical seizures and other abnormal activities, by two experimenters blinded to the genotype and sex. Careful comparison of any EEG abnormality with the concomitant video allowed to exclude that the abnormality was an artifact, e.g., due to chewing, grooming, scratching or other intense movements of the animal, which can sometimes mimic ictiform EEG activity (Anjum et al., 2018).

Seizure activity in humans affected by loss of function mutation of *Slc13a5* ranges from subclinical to polymorphic clinical seizures (Hardies et al., 2015). Therefore, any kind of deviation from a physiological rodent hippocampal EEG (i.e., normal control EEG activity without any paroxysmal alterations, usually typical theta rhythm with rhythmic slow wave activity, 6–9 Hz [Twele et al., 2017]) that could not be verified as an artifact was noted (see Results). The severity of electroclinical seizures was rated by a modified Racine scale (Racine, 1972), in which score 1 was behavioral arrest (associated with paroxysmal EEG activity), score 2 was myoclonic activity (with paroxysmal EEG activity), and score 5 was generalized convulsive seizure activity (with paroxysmal EEG activity).

2.4. Pentylenetetrazole (PTZ) seizure threshold

Thirteen wildtype (*Slc13a5*$^{+/+}$), 14 heterozygote (*Slc13a5*$^{+/-}$), and 12 knock out (*Slc13a5*$^{-/-}$) mice were used for seizure threshold determination. The threshold for PTZ-induced seizures was determined by timed intravenous (i.v.) infusion of a 1% solution of PTZ via flexible tubing placed into the tail vein of mice at a rate of 0.3 ml/min with an infusion pump (Syringe Infusion Pump 22, Harvard Apparatus) as described previously (Töllner et al., 2016). All PTZ seizure threshold determinations were performed at the same time of the day (8 am to 1 pm).

2.5. Behavioral tests

At the age of 10 to 12 weeks all mice underwent all behavioral tests described in the following at the same sequence of tests. The sequence of tests was organized from the least to the most aversive, with an inter-test interval of usually 1 week. Overall, the various tests were performed over a period of four weeks. All behavioral tests were carried out under artificial light and controlled conditions of temperature (22 ± 0.5 °C) and humidity (55 ± 5%). For each of the in vivo tests performed, all animals were tested at the same time of the day, i.e., Morris water maze, and novelty-induced hypophagia were performed in the morning (8 am to 1 pm); Irwin Screen and rotarod were carried out in the afternoon (1 to 4 pm).

A modified version of the Irwin observation test (Irwin, 1968), which comprises a battery of single tests evaluating general health, physiologic parameters and reflexes, and neuronal and behavioral abnormalities (for details see Klee et al. (2015), was used as a screen to evaluate alterations in behavior and physiological function in 15 wildtype (*Slc13a5*$^{+/+}$) and 15 knock out (*Slc13a5*$^{-/-}$) mice. In a modified hanging wire test (Coughenor et al., 1977) for evaluating balance and catalepsy, mice were put upon a grid, which was rotated by 180° with a cut-off after 5 s. Each measure was scored using a rating system from score 0 up to 5 with score 2 representing "normal" appearance, behavior or reaction. Motor performance impairment was also assessed in the rotarod test (Dunham and Miya, 1957) where mice had to walk on a turning rod (6 rpm) for 60 s.

The Morris water maze test (Morris, 1984), in which rodents learn to escape from water onto a hidden platform, was used to evaluate visual-spatial memory and hippocampal integrity in 15 wildtype (*Slc13a5*$^{+/+}$) and 15 knock out (*Slc13a5*$^{-/-}$) mice as described previously (Müller et al., 2009).

The conflict between exploratory behavior and anxiety was assessed in the novelty-induced hypophagia test (Bodnoff et al., 1988; Shephard and Broadhurst, 1982), which measures the diminished feeding behavior of rodents in response to a novel environment. In the present study, the mice were fed with palatable snacks in their home cages for seven consecutive days. For the test day, 16 wildtype (*Slc13a5*$^{+/+}$), 16 heterozygote (*Slc13a5*$^{+/-}$), and 14 knockout (*Slc13a5*$^{-/-}$) mice were placed into a white illuminated square arena (60 × 60 cm, 150–180 lx in corners/center) with a palatable snack in the center. The area was further divided into an inner zone (36 × 36 cm) and an outer zone. The software Ethovision was used to track animals and to analyze parameters such as the latency to consume the palatable snack, velocity, distance moved, time spent in the different zones. Grooming, rearing, urine and defecation were counted manually by two experimenters blinded to the treatment.

2.6. Brain histology

To detect any obvious alterations in morphology and histology of brain regions in *Slc13a5*$^{-/-}$ mice, particularly in the hippocampus, from which EEG recordings had been performed, thionin staining was performed. At the end of the in vivo experiments, the mice were anesthetized and perfused with paraformaldehyde. Series of coronal brain sections (40 µm) were prepared for histology as described previously (Bröer et al., 2016). To analyze differences in myelination, Luxol Fast Blue (LFB) staining on coronal 12 µm cryo-slices of the brain from mice used for CSF sampling were performed. Littermate *Slc13a5*$^{+/+}$ mice were used for comparison.

2.7. In-vitro electrophysiology

To gain initial insights into the mechanisms of SLC13A dysfunction, we undertook investigations in neuronal excitability changes on the cellular and network level, using in vitro measurements in hippocampal brain slices. These were performed in slices from 3 *Slc13a5*$^{-/-}$ mice, and 4 age-matched controls, as well as from 21 Wistar rats (Janvier labs), in the latter case with and without pharmacological blockade of the SLC13A5 transporter using PF-06761281 (2 µM; Sigma Aldrich; cf., Huard et al. (2016) to mimic transporter knockout functionally.

2.7.1. Brain slice preparation and maintenance

The animals were deeply anesthetized by diethyl ether inhalation (Mallinckrodt Baker, Deventer, Netherlands) and decapitated. The brain was quickly removed and transferred into ice-cold (4 °C) and oxygenated (carbogen 95% O_2/ 5% CO_2) dissection solution containing (in mM) 87 NaCl, 25 $NaHCO_3$, 2.5 KCl, 1.25 NaH_2PO_4, 0.5 $CaCl_2$, 7 $MgCl_2$, 10 D-glucose and 75 sucrose adjusted to pH 7.4 with an osmolarity of 326–328 mosmol/l H_2O. The brain was glued to a vibratome (Integraslice 7550 MM, Campden Instruments Ltd., England) and transversal slices of hippocampal formation (400 µm) were prepared in chilled and oxygenated artificial cerebrospinal fluid (aCSF). ACSF was comprised of (in mM) 124 NaCl, 26 $NaHCO_3$, 3 KCl, 1.25 NaH_2PO_4, 2.5 $CaCl_2$, 1.5 $MgCl_2$ and 10 D-glucose adjusted to pH 7.4 with an osmolarity of 304–312 mosmol/l H_2O. After preparation, slices were transferred into a submerged-type storage chamber for maintenance with oxygenated aCSF and kept for 1.5 h, before transferring slices to an

interface-type recording chamber (BSC-BU, Harvard Apparatus Inc., Holliston, MA, USA). During recording, slices were perfused aCSF at 32 ± 1 °C with a continual flow of 2–3 ml/min.

2.7.2. Field potential (FP) recordings of input-output curves and epileptiform activity

FP were recorded in stratum radiatum of the CA1 subfield using borosilicate glass pipettes (GB150-8P Science Products GmbH, Germany) with a tip resistance of 2–3 MΩ (pulled with PIP5 puller from HEKA Elektronik, Lambrecht, Germany) and filled with aCSF containing an Ag/AgCl wire. Signals were amplified and low-pass filtered at 1 kHz (EXT-10-2F, npi electronic GmbH, Germany). Recordings were digitized (Micro 1401mkII, CED Ltd., Cambridge, England) and analyzed using Signal 2.16 (CED Ltd., Cambridge, England). For electrical stimulation, Schaffer collaterals were stimulated with a bipolar platinum electrode composed of twisted insulated platinum wire (PT-2 T, Science Products GmbH, Hofheim am Taunus, Germany). Stimulation was controlled by a Master-8 pulse stimulator (A.M.P.I., Jerusalem, Israel) connected to a stimulus isolator (A365, WPI Inc., Sarasota, FL, USA), applying a paired-pulse protocol with 40 ms inter-pulse interval (IPI) and an inter-stimulus interval (ISI) of 30 s (0.033 Hz). Baseline stimulation strength of each slice was stepwise increased, generating an input-output curve until saturation of amplitude of field excitatory postsynaptic potentials (fEPSP). To induce spontaneous recurrent epileptiform discharges (REDs), Mg^{2+} was omitted from the bath solution. To gauge intensity of epileptiform activity, the number of REDs occurring in 30 s intervals was counted. Likewise, the number of spikes / afterdischarges was counted in all REDs during the last five minutes, and then averaged for each slice. From these averages, the means were obtained for Slc13a5$^{-/-}$ and normal tissues.

2.7.3. Intracellular recordings of active and passive membrane properties

Membrane potential recordings were obtained from CA1 pyramidal neurons with 3 M potassium-acetate-filled (60–120 MΩ) micropipettes, and amplified using a SEC10 amplifier (npi, Tamm, Germany).

2.8. Cerebrospinal fluid (CSF), plasma and brain tissue sampling

For proteomic and metabolomic analysis CSF, plasma and brain tissue were sampled from the same male *Slc13a5*$^{-/-}$ and their littermate controls (*Slc13a5*$^{+/+}$) with an age of 12 weeks. Animals were deeply anesthetized by ketamine/xylazin and blood was drawn by heart puncture. Under stereo-microscope the skin was cut and ***musculus biventer cervicis*** and ***musculus rectus capitis dorsalis major*** were prepared to see the cisterna magna. Puncture of the cisterna magna was performed with a Hamilton syringe to extract 7 to 10 µl CSF per animal (Liu and Duff, 2008). To sample brain tissue mice were sacrificed by cervical dislocation and brain were extracted and hippocampus and parahippocampal cortex were prepared.

2.9. Proteome analysis of hippocampus and parahippocampal cortex

Snap frozen tissue samples were directly bead milled with a Precellys homogenizer (Peqlab, Lutterworth, U.K.) in extraction buffer (10 mM Tris-HCl pH 7.6 with 1% NP40, 10 mM NaCl and Complete protease inhibitors) as described (Molin et al., 2015) and total protein content was measured by Bradford. 10 µg total protein per sample were digested using a modified filter-aided sample preparation (FASP) method as described (Lepper et al., 2018). Proteomic profiling was performed on a Q Exactive HF mass spectrometer (ThermoFisher Scientific, Dreieich, Germany) operated in the data independent acquisition (DIA) mode as described (Lepper et al., 2018). Briefly, 1 µg of peptides per sample were spiked with 1 injection unit of the HRM Calibration Kit (Biognosys, Schlieren, Switzerland, #Ki-3003) for retention time indexing and automatically loaded onto the UPLC system (Ultimate 3000, Dionex, Sunnyvale, CA) equipped with a nano trap column (300 µm inner diameter × 5 mm, packed with Acclaim PepMap100 C18, 5 µm, 100 Å; LC Packings, Sunnyvale, CA). After 5 min, the peptides were eluted from the trap column and separated by reversed-phase chromatography (Acquity UPLC M-Class HSS T3 Column, 1.8 µm, 75 µm × 250 mm; Waters, Milford, MA) using a gradient of 7–27% ACN at a flow rate of 250 nL/min over a period of 90 min, followed by a two short gradients of 27–41% ACN (15 min) and 41–85% ACN (5 min). After 5 min at 85% ACN, the gradient was set back to 3% ACN over a period of 2 min and allowed to equilibrate for 8 min. All ACN solutions contained 0.1% FA.

The DIA method consisted of alternating MS full scans at 120000 resolution ranging from 300 to 1650 *m/z* followed by 37 DIA window scans for peptide fragmentation with a variable width spanning from 300 to 1650 m/z at a resolution of 30,000. Normalized collision energy was set to 28, and the spectra were recorded in profile type.

The DIA LC − MS/MS raw files were converted with HTRMS converter and analyzed using Spectronaut (Version 11, Biognosys, Schlieren, Switzerland) as described (*91*). Briefly, automatic calibration mode was selected with precision indexed retention time (iRT) alignment enabled for applying the nonlinear iRT calibration strategy. Peptides were identified by comparison to an in-house accumulated spectral library from mouse brain samples measured on the same mass spectrometry set-up in a data-dependent acquisition mode. Peptide identification was filtered to satisfy a FDR of 1%. Only proteotypic peptides were considered for protein quantification applying summed precursor quantities based on MS2 area quantity. A match between runs was enabled with the data filtering function set to q-value percentile mode applying a 25% setting. This setting allows only peptide precursor signals passing the 1% FDR threshold in at least 25% of all samples to be considered for identification and quantification aiming to reduce false positive identifications. Evaluation of differential protein abundance between groups was performed by an unpaired Student's *t*-test based on the log2 transformed sum of abundances of all unique peptides per protein.

For the Pathway analysis in each region the protein abundances were subjected to a Pathway enrichment analysis using both a licensed (Genomatix Pathway System (GePS), Genomatix Software GmbH, Munich, Germany) and a publically available pathway tool (ConsensusPathDB over-representation tool (Kamburov et al., 2009). Using both databases a list of all identified proteins was used as a background list. Only pathways with a p value of < 0.01 and at least two overlapping proteins were considered. Protein abundances of all proteins found to be involved in significantly changed pathways were visualized in a heat map. Individual fold changes for each animal were calculated by dividing their value against the mean of the wildtype group, these changes were log2 transformed and the resulting matrix was visualized with the “heatmap.2” function in the “gplots” R package (Warnes et al., 2015) using R version 3.5.1 (R Core Team, 2013).

2.10. Metabolome analysis of cerebrospinal fluid, plasma and brain

Metabolite extraction of CSF (7 µl), plasma (5 µl), and brain tissue (10 mg) was performed using MeOH, CHCL3, and water with a ratio of 2:2:1 for plasma and CSF and 1:2:1 for tissue, respectively. Isotope internal standards were added to CSF, plasma, and weighted preground tissue for absolute quantification of metabolites. Plasma and CSF extracts were vortexed for 10 min at 4 °C and tissues were homogenized using a Retsch mill for 5 min at 30 I/S. Extracts were then centrifuged at 16,000 ×*g* for 5 min at 4 °C and the upper aqueous phase was evaporated and used for metabolite analysis.

Metabolite derivatization and GC–MS analysis was performed as previously described (Cordes and Metallo, 2019). In short, metabolite derivatization was performed using a Gerstel MPS with 15 µl of 2% (*w/v*) methoxyamine hydrochloride (Thermo Scientific) in pyridine (incubated for 60 min at 45 °C) and 15 µl *N*-tertbutyldimethylsilyl-*N*-methyltrifluoroacetamide (MTBSTFA) with 1% *tert-*

butyldimethylchlorosilane (Regis Technologies) (incubated further for 30 min at 45 °C). Derivatized samples were analyzed by using a DB-35MS column (30 m × 0.25 i.d. x 0.25 μm) installed in an Agilent 7890B gas chromatograph (GC) interfaced with an Agilent 5977A mass spectrometer (MS) operating under electron impact ionization at 70 eV. The MS source was held at 230 °C, the quadrupole at 150 °C and helium was used as carrier gas. For MTBSTFA derivatized samples, the GC oven was held at 100 °C for 2 min, increased to 300 °C at 10 °C/min, and held at 325 °C for 3 min. For absolute quantification of citrate and amino acids, a ^{13}C, ^{15}N labeled amino-acid mixture (Cambridge isotope laboratories, Cat. No MSK-A2–1.2) and [2,4-^{13}C]citrate were used as an internal standards. Details on specific fragments are provided elsewhere (Cordes and Metallo, 2019).

2.11. Statistical analysis

Sample size was set based on power analysis calculations using GPower to provide power greater than 0.80 for $\alpha = 0.05$ for most experiments. Except otherwise indicated, all studies were blinded at the level of data analysis. Data from the Morris water maze were analyzed by two-way ANOVA with *posthoc* comparisons by Tukey's multiple comparisons test. For comparison of frequencies in a 2 × 2 table, Barnard's unconditional test (Barnard, 1947) was used, because this test preserves the significance level and generally is more powerful than Fisher's exact test for moderate to small samples (Lydersen et al., 2009).

As with most types of epilepsy in humans, spontaneous recurrent seizures in rodent models are typically infrequent with seizure frequencies of often only 1–2/week and variable inter-seizure intervals (Löscher, 2017). Appropriate statistical models for rare events are based on Poisson random effects models (Johnson et al., 2005; Cai et al., 2010), which was applied here. For analyzing differences in seizure frequency between groups, a Generalized Linear Model with a Poisson error and a log-link was used. Due to an extended overdispersion, a quasi-likelihood approach using a Quasi-Poisson model to account for this was adopted as additional model. These models were performed with R (version 3.4.0; R Core Team (2013)).

Electrophysiological experiments were analyzed using ANOVA to compare passive intracellular properties, and Mann-Whitney Rank Sum Test for comparison of fEPSP slopes. The temporal development of RED-frequency during 0-Mg^{2+} washout was compared with Kolmogorov-Smirnov-Test. These analyses were performed with SigmaStat 3.5.

All other statistical analyses were performed with the Prism 8 software from GraphPad (La Jolla, CA, USA). All tests were used two-sided; a $p \leq .05$ was considered statistically significant.

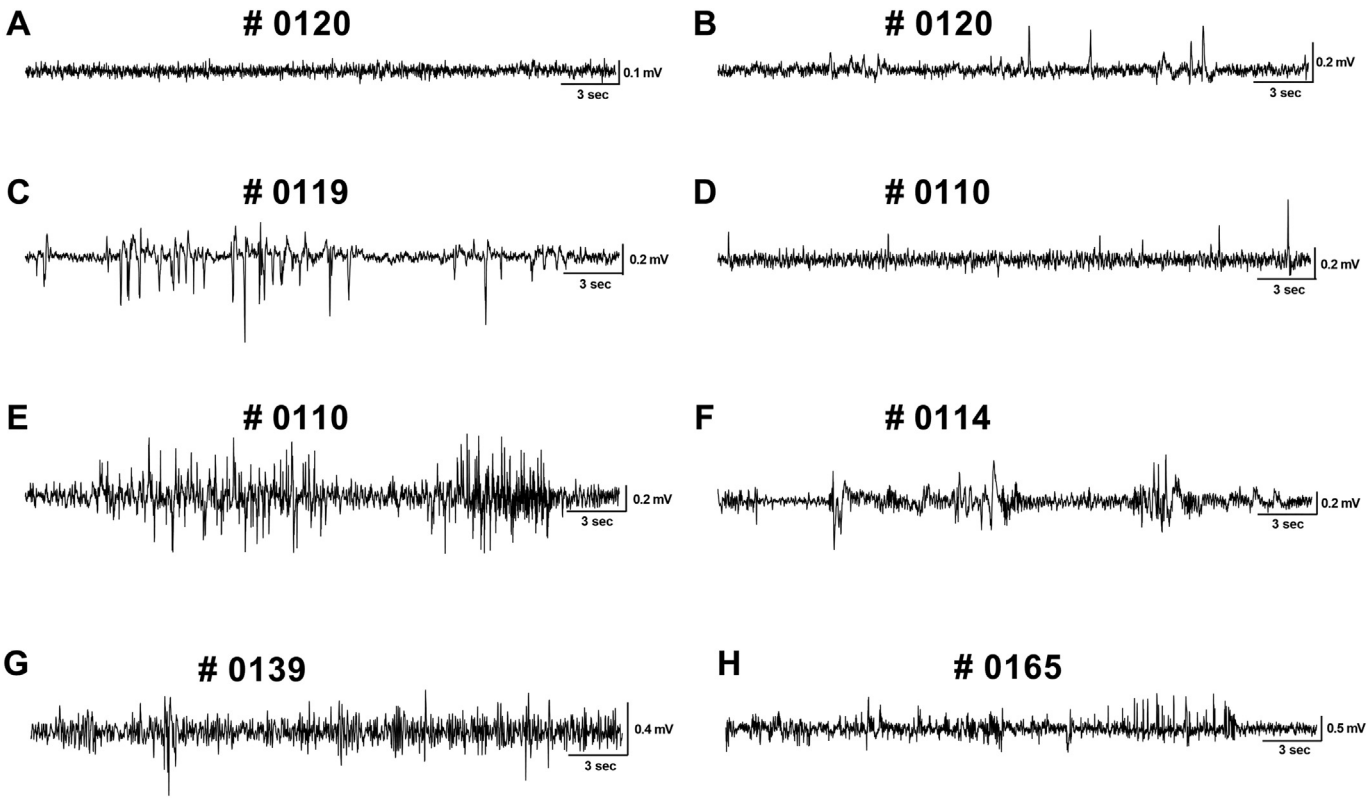

Fig. 1. Representative intrahippocampal EEG recordings in *Slc13a5*$^{+/+}$ and *Slc13a5*$^{-/-}$ mice. The code number of individual mice is indicated above each recording and refers to the numbers given in Table 1, Table S5 and text. (A) Normal baseline activity without any paroxysmal alterations in a *Slc13a5*$^{+/+}$ mouse. Higher magnification showed the typical theta rhythm (rhythmic slow wave activity, 6–9 Hz) occurring in hippocampal recordings of mice. The baseline activity did not differ in *Slc13a5*$^{-/-}$ mice (not shown). (B) Isolated spikes in the hippocampal EEG of a *Slc13a5*$^{+/+}$ mouse. (C) Paroxysmal EEG activity characterized by an irregular, high-amplitude cluster of spikes, associated by myoclonic twitches in a *Slc13a5*$^{+/+}$ mouse. (D) Isolated spikes in the hippocampal EEG of a *Slc13a5*$^{-/-}$ mouse. (E) Paroxysmal high-amplitude run of spikes, during which the *Slc13a5*$^{-/-}$ mouse exhibited behavioral arrest, resembling limbic (focal nonconvulsive) seizure. (F) Paroxysmal EEG activity, characterized by polymorphic high-amplitude spikes and sharp waves, during which the mouse started to twitch, then stretched and flipped over, resembling a generalized convulsive seizure. (G) Paroxysmal EEG activity, lasting about 60 s and characterized by irregular spiking, with low- and high-amplitude spikes, during which behavioral arrest could be observed in a *Slc13a5*$^{-/-}$ mouse. (H) Paroxysmal EEG activity characterized by irregular, low- and high-amplitude run of spikes, which were associated by myoclonic twitches in a *Slc13a5*$^{-/-}$ mouse. Please note that 30 s of EEG are shown for each animal here. Also note the different amplitudes (in mV) of the recordings. The same EEG recordings with higher time-resolution (but only 10 s duration) are shown in Fig. S1. Furthermore, representative examples of the electroclinical seizures recorded in *Slc13a5*$^{+/+}$ and *Slc13a5*$^{-/-}$ mice are shown in movies S1-S4.

3. Results

3.1. Deletion of citrate transporter SLC13A5 leads to epileptic seizures but no obvious behavioral or histological abnormalities in mice

As described in the introduction, patients with homozygous or compound heterozygous loss-of-function mutations in the citrate transporter *SLC13A5* suffer from severe seizure activity and other accompanying clinical signs of epilepsy and encephalopathy, whereas heterozygous carriers are not affected. However, in studies focusing on e.g. liver function (Birkenfeld et al., 2011), our mouse model did not show any obvious neurological alterations. Because of the recent clinical findings regarding SLC13A5-associated human epilepsy, we performed a more detailed neurological investigation in *Slc13a5*$^{-/-}$ mice. For continuous (24/7) video-EEG monitoring, *Slc13a5*$^{-/-}$ mice and littermate heterozygote (*Slc13a5*$^{+/-}$) mice as well as littermate controls (*Slc13a5*$^{+/+}$) of both sex were used, starting at about 7 weeks of age. Body weight of the male and female *Slc13a5*$^{-/-}$ mice used in our experiments was significantly (15–20%) lower compared to controls, confirming previous data (Table S2) (Birkenfeld et al., 2011). The difference in body weight has been explained by a reduction in body size without changes in body composition in young normally fed mice (Birkenfeld et al., 2011).

A total of 2688 h of video-EEG recordings were visually analyzed for occurrence of spikes, electrographic or electroclinical seizures and other abnormal epileptiform activity by experienced observers. In case of any abnormal EEG activity, which was recorded by a depth electrode in the hippocampus, the concomitant video was viewed for behavioral alterations. Based on commonly used definition of seizures (Fisher et al., 2014), an electroclinical seizure was defined as paroxysmal EEG alteration associated by abnormal convulsive or nonconvulsive behavioral alterations with a duration of at least 10 s.

"Normal" baseline EEG activity did not differ between *Slc13a5*$^{+/+}$ and *Slc13a5*$^{-/-}$ mice (Fig. 1A). In both groups, the hippocampal EEG was characterized by typical theta oscillations (6–9 Hz). See Fig. S1 for records with higher time-resolution.

However, EEG spikes or spike clusters were noted in 5 of 8 *Slc13a5*$^{+/+}$ and 7 of 8 *Slc13a5*$^{-/-}$ mice (Fig. 1B and D) at irregular intervals. Such activity may occur in "normal" control mice with depth electrodes, possibly as a result of the damage produced by the electrode (Twele et al., 2017). Abnormal, epileptic EEG activity was detected in 1 of 8 *Slc13a5*$^{+/+}$ and 4 of 8 *Slc13a5*$^{-/-}$ mice (p = .1363; Fig. 1; Table 1; Fig. S1). In the *Slc13a5*$^{+/+}$ mouse #0119 (Fig. 1C), this EEG activity was observed twice on one day during the 2 week-recording period. The abnormal EEG activity was characterized by an irregular, high-amplitude spike cluster lasting about 15 s. This was associated with myoclonic twitches and jumping during running through the cage (Movie S1). In the 4 *Slc13a5*$^{-/-}$ mice with epileptic EEG activity, EEG abnormalities and associated clinical alterations were as follows: Mouse #0110 (Fig. 1E) exhibited six periods of paroxysmal EEG activity, lasting about 20 s each and characterized by high-amplitude run of spikes, during which the mouse showed either behavioral arrest or myoclonic activity (Table 1; Movie S2). Mouse #0114 (Fig. 1F) exhibited two periods of paroxysmal EEG activity, lasting about 20 s and characterized by polymorphic high-amplitude spikes and sharp waves, during which the mouse started to twitch, then stretched and flipped over, resembling a generalized convulsive (stage 5) seizure (Movie S3). Mouse #0139 (Fig. 1G) exhibited three periods of paroxysmal EEG activity, lasting about 60 s and characterized by irregular spiking, with low- and high-amplitude spikes, during which the mouse exhibited behavioral arrest, resembling a limbic (focal nonconvulsive) seizure (as also exhibited by mouse #0110 in Movie S2). Mouse #0165 (Fig. 1H) exhibited one period of paroxysmal EEG activity, lasting about 30 s and characterized by an irregular, low- and high-amplitude run of spikes, which was associated by myoclonic twitches (Movie S4).

Overall, only two periods of seizure-like epileptic EEG activities were observed in one *Slc13a5*$^{+/+}$ mice compared to 12 such activities in four *Slc13a5*$^{-/-}$ mice, including two convulsive (stage 5) seizures in one *Slc13a5*$^{-/-}$ mouse (Table 1). The severity of the observed seizures and cumulative seizure severities are shown in Table 1. The circadian distribution of the paroxysmal EEG activities and seizures varied. Interictal spikes as shown in Fig. 1D were observed in-between the epileptic EEG events. Statistical analysis of the seizure frequencies in *Slc13a5*$^{-/-}$ vs. *Slc13a5*$^{+/+}$ mice by a Generalized Linear Model with a Poisson error and a log-link resulted in a significant difference between groups (p = .0190). On the original scale this was equivalent to an incident rate of 6.00 (95% CI, 1.64 to 38.56). These effects were also recognized within the Quasi-Poisson approach where *Slc13a5*$^{-/-}$ mice compared to wildtype mice are expected to have a rate 6.00 times greater for the number of seizures, but due to a restricted sensitivity of this model with no statistical significance (p = .162).

To test if *Slc13a5* deficiency in mice results in altered seizure susceptibility, seizure threshold was determined by the timed i.v. PTZ infusion test. PTZ seizure thresholds did not significantly differ between the different genotypes (Table S3). The only significant difference was that the maximum seizure severity was higher in female *Slc13a5*$^{-/-}$ mice (5.5 ± 1.6) vs. female *Slc13a5*$^{+/+}$ mice (3.4 ± 0.5; p = .0163). The number of animals which did not survive the seizures did not differ significantly (Table S3).

Since patients with *SLC13A5* mutations have developmental delays and impairments in motor function (Thevenon et al., 2014; Klotz et al., 2016; Alhakeem et al., 2018), a set of behavioral tests including Irwin

Table 1
Results of the video-EEG monitoring over 2 weeks in *Slc13a5*$^{+/+}$ and *Slc13a5*$^{-/-}$ mice. Experiments were started at 7 weeks of age.

***Slc13a5*$^{+/+}$ (n = 8)**					***Slc13a5*$^{-/-}$ (n = 8)**				
Mouse # and sex	Seizures			Cumulative seizure severity (score)	Mouse # and sex	Seizures			Cumulative seizure severity (score)
	Incidence of seizures	Number of seizures per mouse	Seizure severity (score)			Incidence of seizures	Number of seizures per mouse*	Seizure severity (score)	
99 ♂	−	0	0	0	107 ♀	−	0	0	0
108 ♀	−	0	0	0	110 ♀	+	6	4 × 1, 2 × 2	8
119 ♀	+	2	2 × 2	4	114 ♀	+	2	2 × 5	10
120 ♀	−	0	0	0	129 ♀	−	0	0	0
123 ♂	−	0	0	0	139 ♂	+	3	3 × 1	3
142 ♂	−	0	0	0	141 ♂	−	0	0	0
163 ♂	−	0	0	0	154 ♂	−	0	0	0
167 ♂	−	0	0	0	165 ♂	+	1	1 × 2	2
Sum	**1/8**			**4**	**Sum**	**4/8**			**23**

*Significantly different from *Slc13a5*$^{+/+}$ mice (p = .0190).

screen and rotarod, Morris water maze, and novelty-induced hypophagia test were performed in the *Slc13a5*$^{-/-}$ mice and controls. In none of the tests obvious alterations in behavior were observed in *Slc13a5*$^{-/-}$ mice (Fig. 2, Table S4). Rotarod performance was comparable for both genotypes and sexes with all but two female *Slc13a5*$^{-/-}$ mice passing the test after one training session. The two female *Slc13a5*$^{-/-}$ mice failed to walk on the turning rod (6 rpm) for 60 s at the second day of testing.

In the Morris water maze a characteristic learning curve was evident in both genotypes (Fig. 2A). The average escape latency significantly decreased over time without a significant group difference between *Slc13a5*$^{-/-}$ mice and *Slc13a5*$^{+/+}$ mice. In the spatial probe on the last day of testing, neither *Slc13a5*$^{+/+}$ nor *Slc13a5*$^{-/-}$ spent significantly more time at the former platform position compared to other quadrants of the water tank (Fig. 2B). No sex differences were observed, so data from both sexes were averaged. Finally the novelty-induced hypophagia test did not reveal any differences between *Slc13a5*$^{+/+}$ and *Slc13a5*$^{-/-}$ mice for the assessed parameters such as total distance moved, velocity, latency to first entry into the center (where the snack was placed), time spent in each zone (center/inner/outer zone), rearing and grooming behavior (Table S4).

Analysis of brain histology by thionin staining and myelin staining by luxol fast blue (LFB) did not show any obvious differences between *Slc13a5*$^{+/+}$ and *Slc13a5*$^{-/-}$ mice (Fig. 3). Most of the mice of both genotypes exhibited hydrocephalic brain alterations, characterized by enlargement of the lateral and third ventricles and the aqueductus mesencephali (for details see Table S5). This was not associated with any obvious neurologic or behavioral alterations in the *Slc13a5*$^{+/+}$ mice (except the two seizures observed in mouse #119). A comparison of the hydrocephalic brain alterations with occurrence of seizures in *Slc13a5*$^{+/+}$ and *Slc13a5*$^{-/-}$ mice did not indicate any obvious relationship (Table S5).

As to be expected, the hippocampal electrode implantation led to focal neurodegeneration or tissue destruction at the electrode implantation site, but no marked signs of focal inflammation or abscess formation were observed. No significant differences were seen between the knockout and wildtype mice at the electrode implantation site in the hippocampus apart from the morphological findings listed in Table S5. We therefore found no obvious histological changes that may explain the epileptic activity observed in the wild-type mouse. Furthermore, no differences were seen between *Slc13a5*$^{-/-}$ that did or did not exhibit epileptic seizures.

3.2. Both deletion and pharmacological blockade of citrate transporter SLC13A5 increase hippocampal CA1 network excitability

To explore the pathomechanism of the epileptic phenotype described in vivo, we investigated hippocampal synaptic/network excitability changes in both Slc13a5$^{-/-}$ tissue, and in normal tissue blocking SLC13A5 pharmacologically. For these experiments we used the in vitro hippocampal slice preparation, which allows for dosage-controlled drug application without variability being introduced by metabolic or blood-brain barrier issues.

First, we were interested in hippocampal network excitability and epileptogenicity. We therefore tested the propensity of *Slc13a5*$^{-/-}$ hippocampal slices to generate epileptiform activity in the acute 0-Mg^{2+} in vitro epilepsy model, which induces recurrent epileptiform discharges (REDs) (Müller et al., 2013; Brehme et al., 2014). Compared to control slices, there was no difference in the frequency of these events (Fig. 4A), at first sight suggesting no network excitability change. However, the latency to first REDs was consistently ~10 min shorter in *Slc13a5*$^{-/-}$ brain tissue than in control (Fig. 4A, $p < .001$), testifying that with dysfunctional transporter, the tissue becomes more readily excitable during Mg^{2+} washout phase. More importantly, although the frequency of REDs was not increased, their morphology clearly was different, since in *Slc13a5*$^{-/-}$ brain tissue REDs manifested polyspikes/afterdischarges (9.87 ± 1.85 spikes; Fig. 4B insets) in 10/12 slices, while in control tissue, only 8/16 slices did so, with significantly less polyspikes/afterdischarges (4.21 ± 1.23 spikes; $P < .05$; Fig. 4B insets). Since such polyspikes / afterdischarges are deemed to be a sign of epileptogenicity (Smith and Dudek, 2001; Wozny et al., 2005), this again indicates that *Slc13a5*$^{-/-}$ brain tissue is intrinsically more epileptogenic.

We next wanted to explore whether this increased excitability in *Slc13a5*$^{-/-}$ mice is also evident in Mg^{2+}-containing ACSF. To test this, we induced field excitatory postsynaptic potentials (fEPSP) in CA1 in normal, i.e. Mg^{2+}-containing ACSF, using afferent Schaffer collateral stimulation at increasing stimulation strengths. As can be seen in Fig. 4 C and D, under these conditions, there was no functional difference between Slc13a5$^{-/-}$ and normal tissue.

Since persistent (constitutive) knockout of a transporter can in

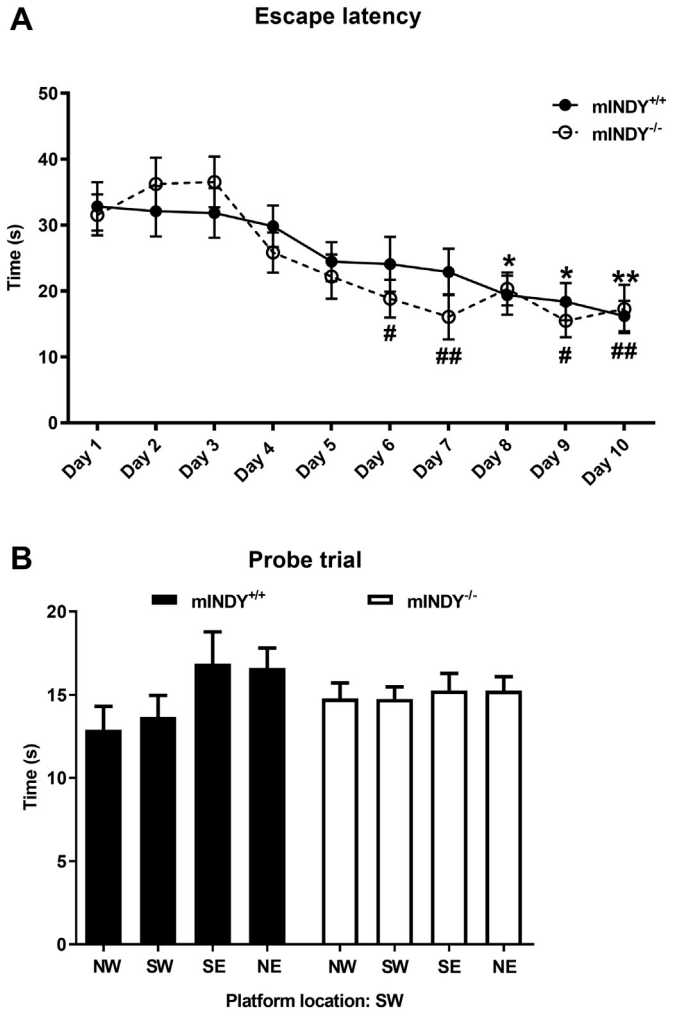

Fig. 2. Learning of platform location by *Slc13a5*$^{+/+}$ and *Slc13a5*$^{-/-}$ in the Morris water maze test. "A" shows the mean time to reach the hidden platform ("escape latency") during the 10 days of water maze testing (acquisition period). Each day, the mice were subjected to four 1-min trials in the maze, and the data of the four trials per day were averaged for each mouse. Both genotypes showed significant learning over the period of the trials. Significant differences to day 1 in *Slc13a5*$^{+/+}$ mice are indicated by asterisk (*$p < .05$; **$p < .01$), while significant differences to day 1 in *Slc13a5*$^{-/-}$ mice are indicated by the hash sign ($^{\#}p < .05$; $^{\#\#}p < .01$). "B" shows the results of the probe trial (day 10, 4th trial), in which the platform was removed and the crossings of the former platform position during a single trial over 60 s were recorded. Neither *Slc13a5*$^{+/+}$ nor *Slc13a5*$^{-/-}$ spent significantly more time at the former platform position compared to other quadrants of the water tank. In both graphs, data are presented as means ± SEM of 10 mice per genotype.

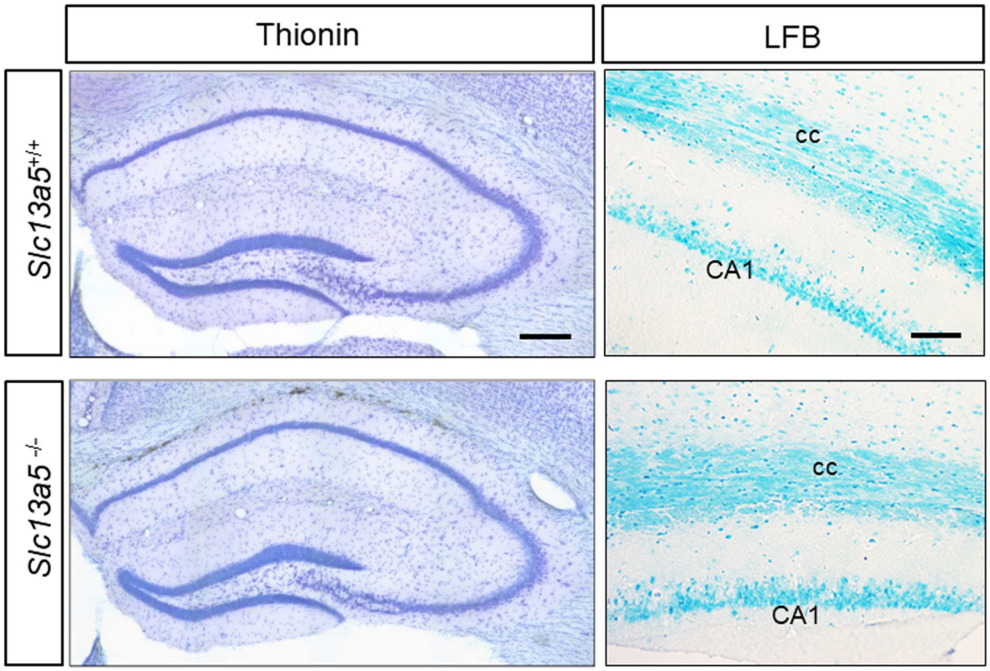

Fig. 3. Representative photomicrographs of thionin-stained (left) and luxol fast blue-stained (right) brain sections of a *Slc13a5*$^{+/+}$ and a *Slc13a5*$^{-/-}$ mouse. No neuronal abnormalities in hippocampal formation and parahippocampal areas or changes of neuronal myelination of *Slc13a5*$^{-/-}$ were observed. Note the ventricle enlargement in both mouse genotypes (see Table S5 for details). Cc = corpus callosum; CA1 = cornu ammonis 1. Scale bar left = 200 μm. Scale bar right = 100 μm. (For interpretation of the references to color in this figure legend, the reader is referred to the web version of this article.)

principle activate adaptive changes during development, the above-described excitability increases in *Slc13a5*$^{-/-}$ tissue could be due to such adaptive plasticity. Thus, to confirm the involvement of SLC13A5 transporter in the control of network excitability in a general way, we investigated the effects of pharmacological SLC13A5 transporter block using the specific antagonist PF-06761281 (2 μm) in normal rodent (now rat) hippocampal tissue in a set of experiments mirroring the above, such that adaptive mechanisms due to knockout of the gene and species-specific effects can be ruled out. With respect to PF-06761281, it should be noted that this compound is a dicarboxylate molecule mimicking citrate and potentially having chelating properties as well (Willmes and Birkenfeld, 2013). Therefore, an unspecific effect by the dicarboxylate cannot be ruled out. Additionally, PF-06761281 is also inhibiting astrocyte specific SLC13A3 transporter to a lesser extent, potentially influencing the experiments.

Gauging the severity of hippocampal REDs, we could recapitulate the epileptogenic phenotype also under pharmacological blockade of the transporter, albeit qualitatively different than in *Slc13a5*$^{-/-}$ mouse tissue. Rather than generating more polyspikes/afterdischarges or showing differences in the latency of RED emergence, the frequency of REDs was significantly increased with functionally blocked SLC13A5 (Fig. 4 E,F, $p < .001$), demonstrating that impeded transporter function also using an alternative to knockout is instrumental in shaping network excitability, although in a slightly different fashion.

Analyzing excitatory synaptic responsiveness, we found that under transporter blockade, even normal fEPSPs in CA1 under non-epileptogenic conditions were increased. As can be seen in Fig. 4 G,H, the resulting input-output curve under citrate transporter block was increased significantly ($p = .012–0.032$), indicating that under these conditions also synaptic responsiveness was augmented, too.

As the above hyperexcitability phenomenon could in principle be due to changes in intrinsic or synaptic excitability, we analyzed CA1-neuronal passive and firing behavior, using sharp-microelectrode intracellular recordings (Table S6). Neither input resistance nor time constant were different between the two groups, nor was firing behavior (firing input-output curves not different between the two groups; data not shown). In addition, we tested for differences of intrinsic currents modulating excitability of neurons, i.e., HCN channel-dependent voltage sags at hyperpolarizing current injections, or calcium activated potassium current-dependent after-hyperpolarizations at depolarizing current injections. Neither of the two was different between neurons with and without SLC13A5 block, ruling out that the transporter has any major impact on intrinsic neuronal behavior.

3.3. Proteome analysis indicates alterations in neurotransmitters, extracellular matrix organization and lipid metabolism in the brain of SLC13A5 deficient mice

In order to detect potential changes in protein abundance in *Slc13a5*$^{-/-}$ mice, a quantitative proteomic analysis was performed on hippocampus and parahippocampal cortex tissue using five wildtype and five *Slc13a5*$^{-/-}$ mice. In the hippocampus 5.4% (286 out of 5249) and in the parahippocampal cortex 1.5% (77 out of 5249) of identified proteins showed a significant difference in abundance levels.

In order to obtain information about the regulation of mechanistically linked groups of proteins, we subjected the datasets of differentially abundant proteins to pathway enrichment analysis using two databases, ConsensusPathDB and Genomatix. A total of 30 (ConsensusPathDB) and 3 (Genomatix) regulated pathways were identified in the hippocampus (Table S7A, B). In the parahippocampal cortex, regulation of 59 (ConsensusPathDB) and 9 (Genomatix) pathways was demonstrated (Table S8A, B). With regard to the total number of regulated pathways, it needs to be considered that several of these regulated pathways share the same subset of proteins. Expression levels of all proteins involved in regulated pathways are illustrated in Fig. 5.

In the hippocampus, regulated protein groups that can be directly linked to neuronal activity and its regulation comprised GABA- (e.g. *GABA shunt, GABA synthesis, release, reuptake and degradation of GABA*) and serotonin-related pathways (*metabolism of serotonin, serotonin clearance from the synaptic cleft, and serotonin degradation*). In these pathways, proteins involved in GABA trafficking (STX1A and DNAJC5) and metabolism (ALDH5A1 and ABAT) exhibited significantly lower abundance levels in *Slc13a5*$^{-/-}$ mice. Abundance of glutamate decarboxylase 65 (GAD65; encoded by GAD2), a catalyst for the production of GABA, showed significantly higher levels in knockout mice. The proteins involved in serotonin metabolism and degradation (MAOA and ALDH2) exhibited significantly decreased abundance levels in *Slc13a5*$^{-/-}$ mice.

Analysis of protein expression patterns in the parahippocampal cortex did not reveal significantly over- or underrepresented pathways,

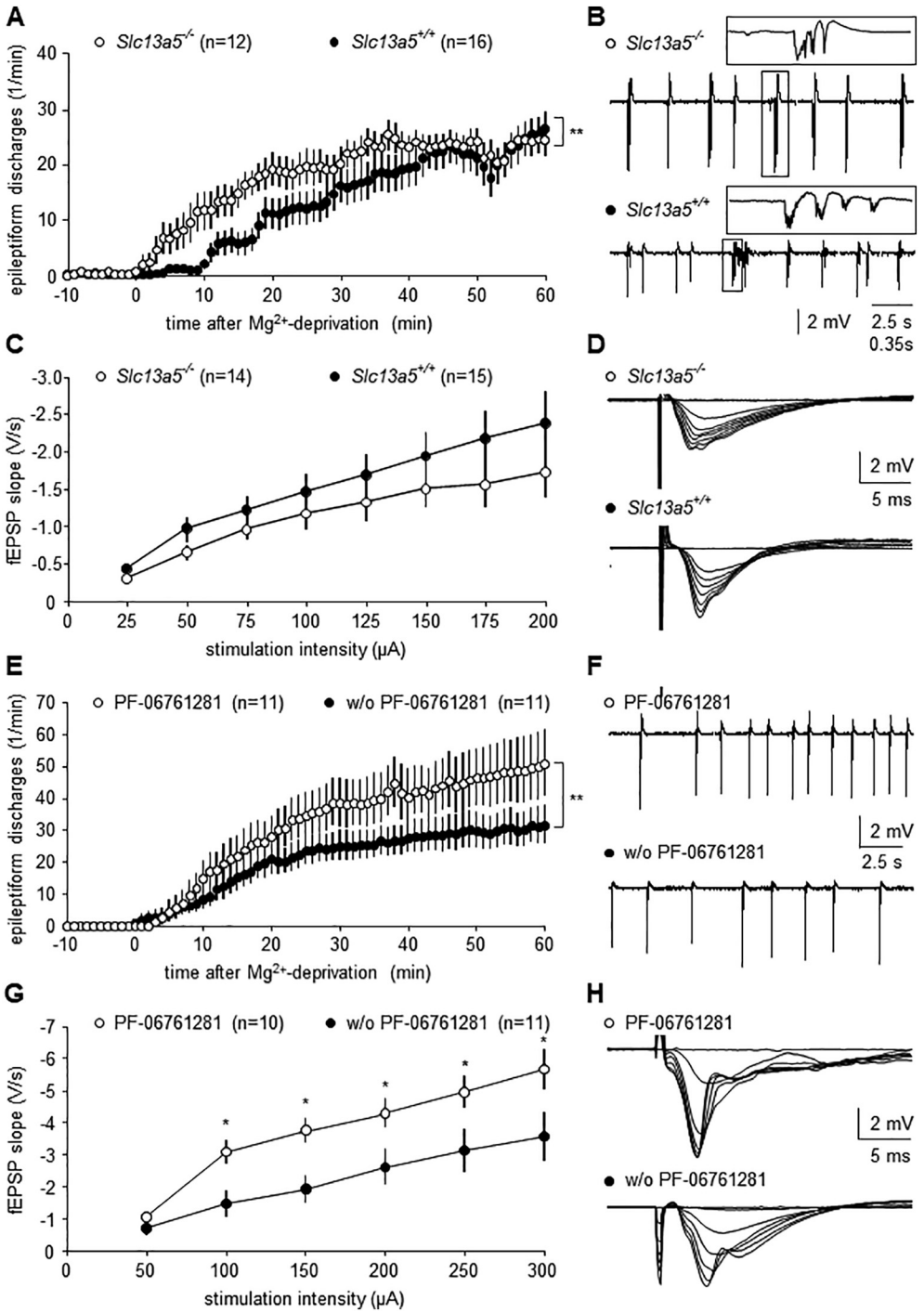

Fig. 4. Effect of the *Slc13a5* knockout (A-D) and of the SLC13A5 inhibitor PF-06761281 (2 µM) (*E*-H) on hippocampal network activity and synaptic transmission of Schaffer collateral-CA1 pyramidal cell synapses. (A) Epileptiform discharges recorded in the stratum radiatum of CA1-region were monitored during perfusion with Mg^{2+}-free ACSF. Note the left-shift of discharge onset of spontaneous epileptiform discharges in *Slc13a5*$^{-/-}$ mouse slices (open circles), as compared to control mouse slices (closed circles). Asterisks: Significant shift, $p < .001$, Kolmogorov-Smirnov-Test. (B) Representative sample traces of REDs illustrating the increased incidence of polyspikes / afterdischarges in knockout tissue (see insets with single discharges enlarged from traces) 60 min after of removal of Mg^{2+}. (C) Input-output curves representing fEPSP slope in response to increasing stimulus input in *Slc13a5*$^{-/-}$ mouse slices (open circles), as compared to control mouse slices (closed circles). (D) Representative traces illustrated by overlaying each fEPSP to stimulus from 0 to 300 µA. (E) Epileptiform discharges recorded in the stratum radiatum of CA1-region in rat slices were monitored during perfusion with Mg^{2+}-free ACSF. Note the significant increase of spontaneous epileptiform discharges in the presence of PF-06761281 (open circles) compared to control experiments without PF-06761281 (closed circles) ($p < .001$, Kolmogorov-Smirnov-Test). (F) Representative sample trace illustrating the occurrence of spontaneous epileptiform activity 60 min after removal of Mg^{2+}. (G) Input-output curves representing fEPSP slope in response to increasing stimulus input with (open circles) and without PF-06761281 (closed circles). (H) Representative traces illustrated by overlaying each fEPSP to stimulus from 0 to 300 µA.

which are directly linked with neuronal activity. However, significant group differences became evident in the abundance of proteins involved in extracellular matrix organization and immune response (in the *il 3 signaling pathway*). In these pathways, protein tyrosine phosphatase, non-receptor type 6 (PTPN6) exhibited the strongest regulation with a pronounced reduction as a consequence of the *Slc13a5* genetic deficiency.

Further regulated pathways do not seem to be directly related to an epileptic phenotype of the *Slc13a5*$^{-/-}$ mice. The significant differential expression of several pathways in the hippocampus indicates differences in metabolic functioning (*respiratory electron transport, complex I biogenesis and oxidative phosphorylation pathways*). The respective proteins proved to be dysregulated with either lowered or increased abundance of mammalian respiratory complex I proteins in *Slc13a5*$^{-/-}$ mice. In the parahippocampal cortex, significant differences in lipid metabolism pathways (*lipoprotein metabolism, HDL-mediated lipid transport and lipid digestion, mobilization, and transport)* were identified with an increased abundance of low density lipoprotein receptor (LDLR) and apolipoprotein A1 (APOA1) in *Slc13a5*$^{-/-}$ mice.

3.4. Deletion of the citrate transporter Slc13a5 leads to altered citrate concentrations in cerebrospinal fluid (CSF) and parahippocampal cortex

Next, we performed metabolomic analyses to examine whether the deletion of the citrate transporter SLC13A5 leads to changes in the composition of organic acids and amino acids in plasma, CSF, and brain

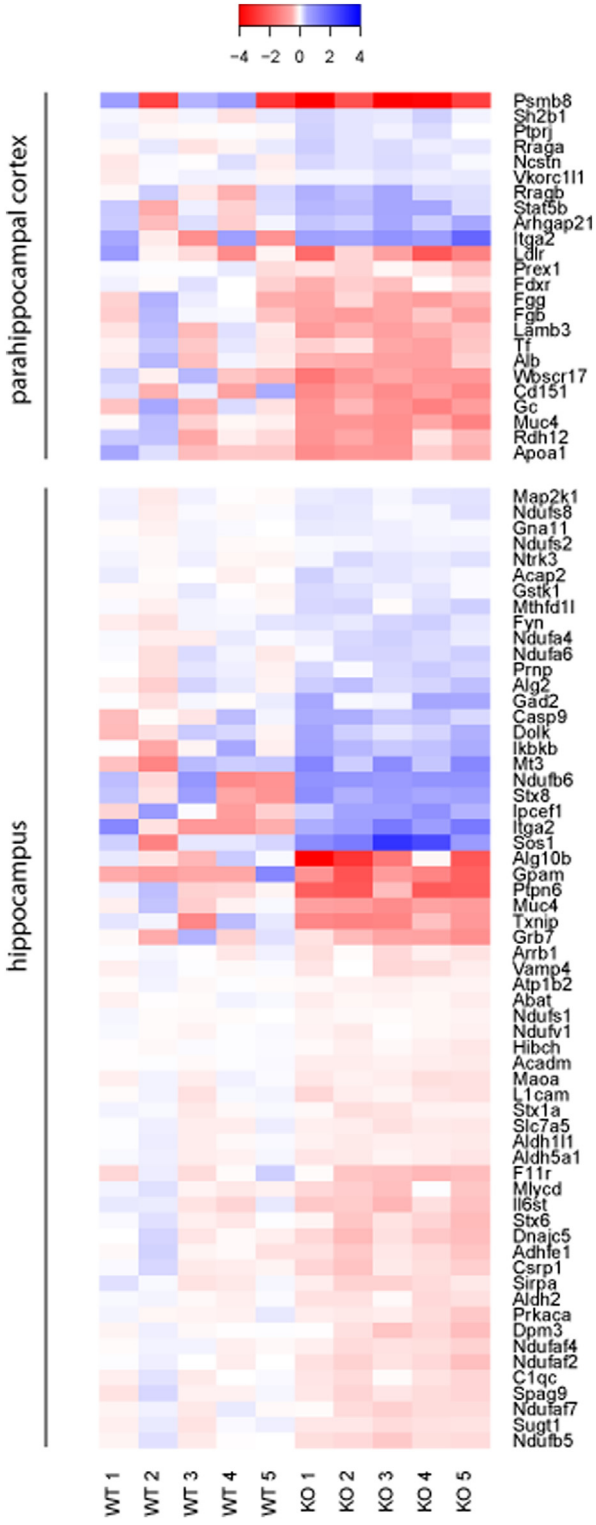

Fig. 5. Expression analysis of proteins for the hippocampus and parahippocampal cortex of 5 wildtype (WT; *Slc13a5*$^{+/+}$) and 5 knockout (KO; *Slc13a5*$^{-/-}$) mice are shown. For hierarchical row clustering protein data was log2 transformed. Red cell color indicates an upregulation, blue cell color a down-regulation. The respective color code is given above the heat map. (For interpretation of the references to color in this figure legend, the reader is referred to the web version of this article.)

tissue. Mice were fasted for 4 h in the morning. Then, plasma, CSF and tissues from the parahippocampal cortex and hippocampus were obtained as described in the Methods section. Samples were analyzed with gas chromatography–mass spectrometry (GC–MS). In plasma, we did not observe any significant change in organic acid levels in *Slc13a5* knockout and wildtype mice (Fig. 6A and Fig. S2 A-C). Therefore, potential changes in CSF or brain might not be explained by systemic changes. In CSF of *Slc13a5*$^{-/-}$ mice, citrate levels were significantly increased (Fig. 6B) compared to *Slc13a5*$^{+/+}$ mice. In apparent contrast, citrate levels were significantly decreased in parahippocampal cortex in *Slc13a5*$^{-/-}$ mice (Fig. 6C). Of note, citrate was markedly lower in CSF than in plasma (Fig. 5A, B) of both, wildtype and knockout mice. Lactate and succinate levels were reduced in CSF of *Slc13a5*$^{-/-}$ mice compared to *Slc13a5*$^{+/+}$ mice (Fig. 6D, E). The amino acids glutamate and aspartate were increased by 34 ± 5% and 29 ± 3%, respectively, in the CSF of *Slc13a5*$^{-/-}$ mice (Fig. 6F, S1). Other amino acids did not differ between *Slc13a5*$^{-/-}$ and *Slc13a5*$^{+/+}$ mice, neither in CSF nor in plasma (Figs. S2 and S3). Beside decreased citrate levels in parahippocampal cortex, no other major changes were observed in the tissue metabolites including GABA and *N*-acetylaspartate (NAA; Figs. S4 – S6).

4. Discussion

The main findings of the present study are summarized in Fig. 7. Using continuous (24/7) video-EEG monitoring as well as ex vivo electrophysiological recordings, our data demonstrate that deletion of *Slc13a5* in a mouse model leads to increased neuronal excitability resulting in increased propensity for epileptic seizures, thus indicating a good face validity of the mouse model. However, during the two weeks of video/EEG monitoring, epileptic seizures were only observed in 50% of mice with deleted *Slc13a5*, which may either indicate a very low seizure frequency in the other 50% of mice or incomplete penetrance of the deletion in the affected animals. Penetrance refers to the likelihood that a clinical condition (or phenotype) will occur when a particular genotype is present. A condition is said to show incomplete penetrance when some individuals who carry the pathogenic variant express the associated trait while others do not, which is also known from other genetic rodent models of epilepsy (Kurtz et al., 2001; Mulley and Mefford, 2011; Italiano et al., 2016; Liu et al., 2019). The penetrance in humans with *SLC13A5* loss-of-function mutation is unknown but none of the individuals with heterozygous mutations show any epileptic phenotypes (Thevenon et al., 2014; Hardies et al., 2015; Klotz et al., 2016; Schossig et al., 2017; Alhakeem et al., 2018).

As reported in patients with *SLC13A5* mutations (Hardies et al., 2015; Klotz et al., 2016), seizure types in *Slc13a5*$^{-/-}$ mice ranged from myoclonic and focal (nonconvulsive), which was observed in the majority of affected mice, to generalized convulsive seizures. Clinical seizures were associated with paroxysmal EEG alterations, which were recorded by depth electrodes from the hippocampus. Unexpectedly, paroxysmal EEG alterations associated with myoclonic twitches and jumping were also observed in one *Slc13a5*$^{+/+}$ mouse, but overall seizure frequency was significantly higher in the *Slc13a5*$^{-/-}$ mice. Furthermore, generalized convulsive seizures were only observed in a knockout mouse. Interestingly, the behavioral arrest (or “freezing”) observed in some of the mutant mice during paroxysmal EEG activity is a typical limbic (or focal) seizure activity also observed in the intrahippocampal kainate model in mice (Riban et al., 2002). Such limbic seizure activity was not observed in *Slc13a5*$^{+/+}$ controls, indicating hippocampal abnormalities in the *Slc13a5*$^{-/-}$ mice. It is important to note that without continuous video-EEG monitoring, most epileptic seizures in *Slc13a5*$^{-/-}$ mice would have been overseen, because generalized convulsive seizures occurred so rarely, and the more frequent limbic or myoclonic seizures are difficult to detect without continuous EEG recording.

In the present study, we recorded seizures by depth electrodes from the hippocampus in vivo. However, this does not necessarily imply that these seizures originated in the hippocampus. Instead, the metabolomic data on parahippocampal cortex vs. hippocampus demonstrate that the

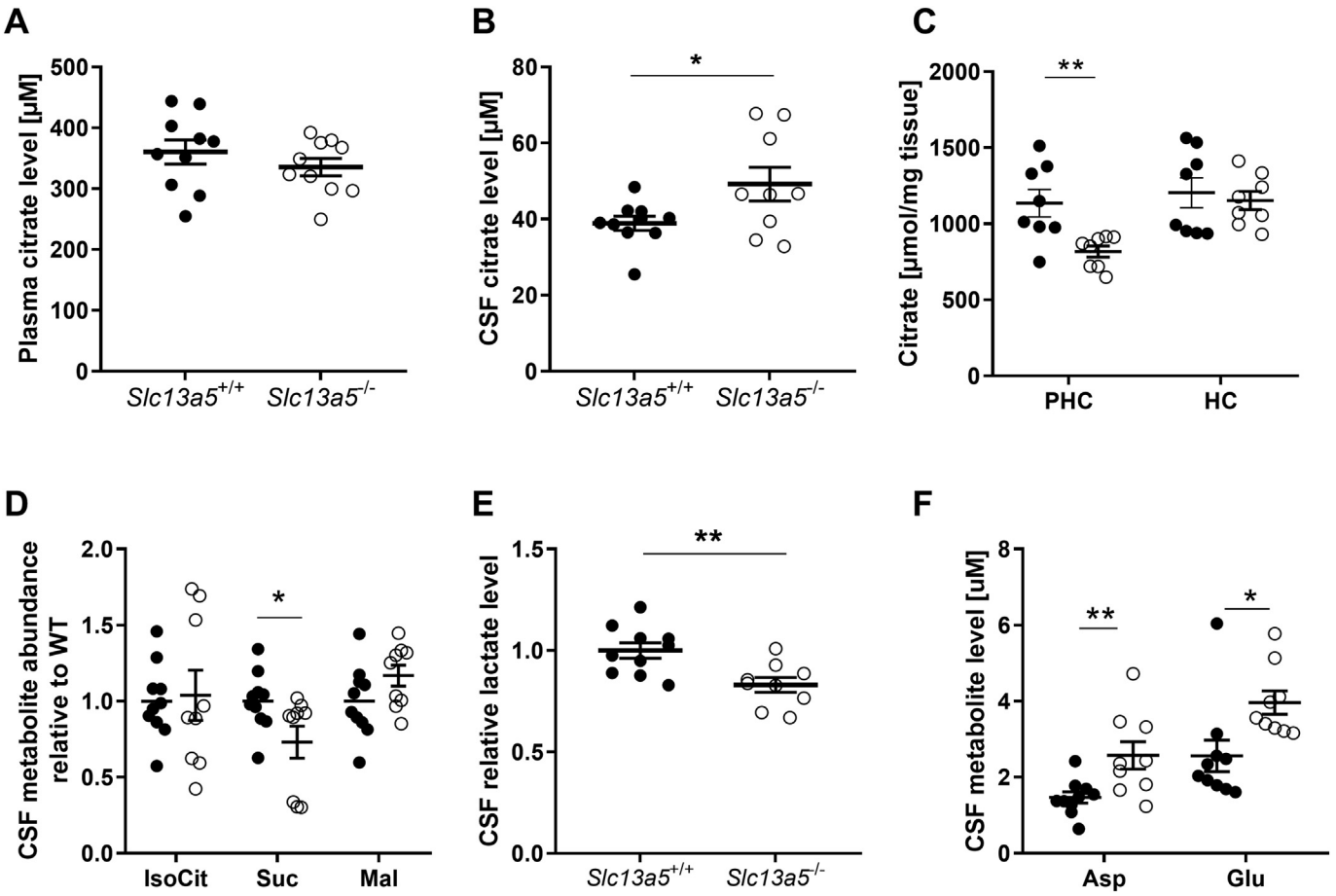

Fig. 6. Citrate, TCA-cycle intermediates and amino acid analysis of CSF and plasma from *Slc13a5*$^{+/+}$ (closed circles) and *Slc13a5*$^{-/-}$ (open circles) were analyzed by GC–MS. (A) Citrate levels are not changed in plasma of *Slc13a5*$^{-/-}$ mice, whereas they are increased in CSF (B). (C) Citrate in parahippocampal cortex (PHC) is significantly decreased in *Slc13a5*$^{-/-}$ mice, but not changed in hippocampus (HC). (D) Succinate as well as lactate (E) are decreased in CSF of *Slc13a5*$^{-/-}$ mice, whereas aspartate and glutamate are increased in CSF (F). Data are shown as mean ± SE;M; *p < .05; **p < .01.

decrease in citrate levels in *Slc13a5*-knockout mice was restricted to the parahippocampal cortex, which may thus constitute a region of seizure onset. Thus by using hippocampal depth electrodes for seizure detection, part of the seizures may have been missed. The parahippocampal region, which surrounds the hippocampus and encompasses a large portion of the medial temporal lobe, including the piriform, perirhinal, and entorhinal cortices, is important in contributing to limbic seizure initiation and epileptogenesis; seizures generated in the parahippocampal cortex propagate to the hippocampus, altering the excitability of hippocampal neurons as seen here (Löscher and Ebert, 1996; Nadel, 2000; Scharfman, 2000; McIntyre and Gilby, 2008).

The present electrophysiological experiments in hippocampal slices suggest that network excitability is significantly increased when the function of the SLC13A5 transporter is infringed. This corroborates the increased seizure susceptibility as shown in the in vivo experiments in *Slc13a5*$^{-/-}$ mice, and further confirms that this is not species specific, since transporter block in rat tissue also induces increased excitability. The hyperexcitability signs are likely due to synaptic, rather than intrinsic neuronal property changes, as the latter are not influenced by transporter dysfunction. Indeed, one may speculate that at least in the knockout tissue, NMDA-receptor-mediated transmission is enhanced, as this has been linked to afterdischarge-generation by other groups previously (Behr et al., 2001). A possible explanation for differences between pharmacological inhibition of SLC13A5 and *Slc13a5* knock-out observed here (see Results) would be compensatory mechanisms during development of the knock-out mice. Irrespective of this, the molecular mechanisms underlying the hyperexcitability change seen in the hippocampal slices of both *Slc13a5*$^{-/-}$ mice and normal rats could include NMDA or AMPA receptor enhancement (Westergaard et al., 2017; Kalappa and Tzounopoulos, 2017) or GABAergic (disinhibitory) mechanisms (Wilkins and Smart, 2002), as any of these receptors has been shown to be modulated by Zn^{2+}, which could in effect be increasingly chelated by ambient citrate (estimated to be around 2.1 mM in hippocampal slices [McDougal Jr. et al., 1997]) due to citrate transporter block (Westergaard et al., 2017).

When determining individual seizure threshold by PTZ infusion, female *Slc13a5*$^{-/-}$ mice exhibited significantly higher seizure severity than female controls, which was not observed in male *Slc13a5*$^{-/-}$ mice, thus indicating a sex difference in the consequences of the *Slc13a5* knockout in mice. This observation seems to be confirmed in the clinical setting (personal communication, Dr. Brenda Porter, Department of Neurology, Stanford University School of Medicine, U.S.), but detailed studies are needed in patients to formally confirm the notion of a higher seizure severity in female subjects.

Other than occurrence of spontaneous seizures or alterations in seizure threshold, *Slc13a5*$^{-/-}$ mice did not show any obvious behavioral or cognitive abnormalities in a battery of behavioral tests. In affected humans, SLC13A5-associated epilepsy is accompanied with developmental delay, slow progression of motor function, variable combinations and degrees of ataxia, choreoathetosis and spasticity, and significant impairment in language and speech development (Bhutia et al., 2017). Whereas the developmental delay may be reflected by the lower body weight gain observed in *Slc13a5*$^{-/-}$ mice, slow progression of motor function or ataxia were not noted in these animals. Phenotypic

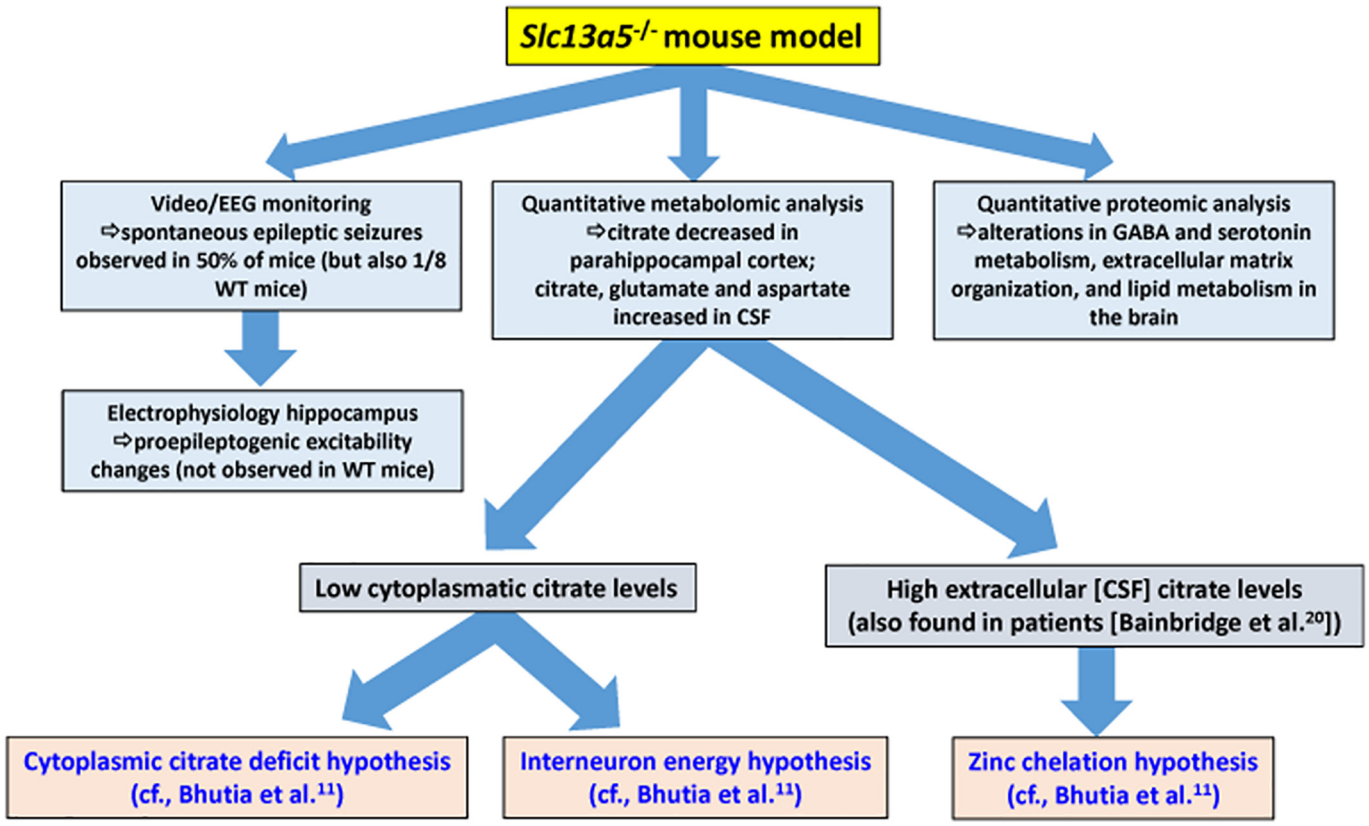

Fig. 7. A summary of the main findings of the present study and how they relate to the suggested hypotheses of Bhutia et al. (*11*).

differences between affected mice and humans may relate to physiologically relevant differences in kinetic features between the human and rodent transporters in that the Michaelis constant for the transporter to transport citrate is ~20 μM in mice, whereas the corresponding value for the human is at least 30-fold higher (Birkenfeld et al., 2011; von Loeffelholz et al., 2017; Willmes et al., 2018). However, it cannot be excluded that other mechanisms, unrelated to SLC13A5, further contribute to the human phenotype.

Histological examination of hippocampus and parahippocampal areas did not disclose any neuronal differences between *Slc13a5*$^{-/-}$ mice and *Slc13a5*$^{+/+}$ controls. However, both mouse genotypes exhibited hydrocephalic brain alterations, which were not associated with any obvious neurologic or behavioral abnormalities in *Slc13a5*$^{+/+}$ controls (except the two seizures observed in mouse #119). However, we cannot exclude that hydrocephalus in *Slc13a5*$^{-/-}$ mice contributed to the phenotypic consequences of *Slc13a5* deletion, although hydrocephalus is not commonly recognized as a cause of seizures (Sato et al., 2001). Congenital hydrocephalus is a relatively frequent observation in genetically engineered mice, particularly when using C57BL background strains, and is often due to dysfunction of motile cilia on ependymal cells (Vogel et al., 2012). To our knowledge, it is not known whether *SLC13A5* mutations in patients are associated with consistent structural brain alterations. Furthermore, as yet no conclusive MRI or other imaging data from affected homozygous patients, heterozygous carriers (who have no noticeable phenotype) and their parents are available. Thevenon et al. (2014) described that brain imaging was not conclusive in seven patients from two families. Klotz et al. (2016) reported that in a group of nine epilepsy patients with *SLC13A5* mutations, MRI was normal in six, while one patient exhibited focal frontal lobe thickening, one patient hyperintense foci in parietal white matter, and one patient focal loss of gray matter, respectively. In another study in eight patients with homozygous or compound heterozygous mutations in the *SLC13A5* gene, six out of seven infants with a neonatal MRI had a characteristic MRI pattern, with punctate white matter lesions, which were no longer visible at the age of 6 months, but led to gliotic scarring visible on MRI at the age of 18 months (Weeke et al., 2017). Hardies et al. (2015) reported MRI findings in two affected siblings, indicating periventricular leukomalacia-like abnormalities, which are known to result in hydrocephalus (Deng et al., 2008).

Virtually nothing is known about the molecular basis for the development of epilepsy in children with loss-of-function mutations in *SLC13A5* except that the association between *SLC13A5* mutations and epilepsy may indicate an obligatory neuronal function for the transporter in the brain (Bhutia et al., 2017). Based on theoretical grounds, Bhutia et al. (2017) have proposed several potential mechanisms (cf., Fig. 7), including the “neuronal cytoplasmatic citrate deficit hypothesis”, the “interneuron energy hypothesis”, and the “zinc chelation hypothesis”. Furthermore, SLC13A5 defects might interfere with neuronal myelination (Bhutia et al., 2017). These hypotheses were addressed in our experiments in *Slc13a5*$^{-/-}$ mice.

In the brain, citrate is released from astrocytes to the extracellular space and is normally transported into the cytoplasm of neurons through the action of SLC13A5 (Sonnewald et al., 1991; Westergaard et al., 1995; Westergaard et al., 2017). Our metabolomic data from GC–MS analysis of plasma, CSF and brain tissue show that deletion of SLC13A5 leads to increased citrate levels in CSF and decreased citrate levels in parahippocampal cortex, suggesting reduced neuronal uptake. Similar to the present findings in *Slc13a5* knockout mice, increased CSF citrate levels have been reported for *SLC13A5* mutant epilepsy patients, supporting the hypothesis that loss of SLC13A5 function alters TCA metabolism and may disrupt metabolic compartmentation in the brain (Bainbridge et al., 2017). Interestingly, citrate injection into the CSF has been shown to induce seizures in rodents, which is inhibited by co-administration of Ca^{2+} (Hornfeldt and Larson, 1990).

In the cytoplasm, citrate controls glycolysis by allosterically inhibiting the rate-limiting enzyme phosphofructokinase-1, thus

suppressing glycolysis (Ros and Schulze, 2013). Yet, this particular function is not likely to be relevant to the pathogenesis of epilepsy, since citrate is expected to decrease in cytoplasm upon deletion of SLC13A5, and not increase. Accordingly, when we deleted the transporter in the liver, we did not observe any decrease in glycolysis in the liver (Birkenfeld et al., 2011). In the brain, metabolic pathways are compartmentalized between astrocytes and neurons, in that astrocytes mainly can activate glycolysis and are limited in TCA cycle whereas neurons can upregulate TCA cycle and oxidative phosphorylation with a limited capacity of glycolysis. Consequently, astrocytes take up glucose and metabolize it to lactate, which is then released into the extracellular space for subsequent uptake by neurons for use in energy production (Magistretti and Allaman, 2015). In the mouse brain, SLC13A5 is expressed both by neurons and astrocytes (Lamp et al., 2011; Pajor, 2014). Our data show increased citrate and decreased lactate levels in CSF of *Slc13a5*$^{-/-}$ mice, which could point to an inhibition of glycolysis by elevated citrate in astrocytes.

Citrate might serve as a significant source of energy in neurons, and NaCT loss of function may induce an energy deficit, similar to the liver (Birkenfeld et al., 2011). Energy deficit in neurons caused by low cytoplasmatic citrate levels in brain parenchyma as found in the present study formed the basis of the interneuron energy hypothesis proposed by Bhutia et al. (2017), because inhibitory interneurons have a higher energy metabolism than principal neurons (Kann, 2016). If an energy deficit is generated in inhibitory neurons through reduced cytoplasmic citrate, the ability of inhibitory neurons to modulate glutamatergic excitation would be impaired, which would result in enhanced seizure susceptibility as observed here.

Deletion or inhibition of SLC13A5, thus inhibiting citrate uptake, has been shown to reduce fatty acid synthesis in hepatocytes and liver tissue (Birkenfeld et al., 2011; Pesta et al., 2015; von Loeffelholz et al., 2017). Citrate is a source of carbon in the biosynthesis of fatty acids and cholesterol, and involved in the generation of the neurotransmitters glutamate and GABA, and in acetylation of histones and non-histone proteins (Iacobazzi and Infantino, 2014; Bhutia et al., 2017). A decrease in the cytoplasmic levels of citrate as a consequence of SLC13A5 deletion or inhibition in the brain may lead to decreased synthesis of fatty acids and cholesterol, which might interfere with neuronal myelination (Bhutia et al., 2017). Yet, our study showed normal myelination patterns in *Slc13a5*$^{-/-}$ mice. Therefore, this explanation seems unlikely to account for the epileptic phenotype associated with *Slc13a5* deletion.

Citrate is a potent chelator of divalent cations, including Mg^{2+} and Ca^{2+}, and particularly Zn^{2+} (Field et al., 1975; Glusker, 1980). The NR2A subunit of the glutamatergic NMDA receptor possesses a high-affinity allosteric binding site for zinc (Paoletti et al., 1997; Amico-Ruvio et al., 2011; Romero-Hernandez et al., 2016). Occupation of this high affinity site by Zn^{2+} has an inhibitory effect on NMDA receptor function. By studying the chelating effects of zinc on NMDA receptor function, it has been reported that co-application of citrate with free zinc enhances NMDA receptor-mediated currents (Westergaard et al., 1995). Therefore, the idea that zinc chelation could potentiate NMDA receptor function at central glutamatergic synapses is a plausible mechanism that could explain how elevated extracellular citrate levels (as indicated by increased CSF citrate levels) may lead to enhanced NMDA receptor-mediated synaptic transmission (Bhutia et al., 2017). Indeed, as discussed above, molecular mechanisms underlying the hyperexcitability change seen in the hippocampal slices of *Slc13a5*$^{-/-}$ mice could include NMDA receptors.

In line with increased glutamatergic transmission, we observed increased CSF concentrations of glutamate and aspartate in *Slc13a5*$^{-/-}$ mice. Glutamate can arise from citrate in the cytoplasm by the sequential actions of aconitase, isocitrate dehydrogenase and transaminases; all of these enzyme activities are present not only in the mitochondrial matrix but also in the cytoplasm. GAD would then convert glutamate into GABA in GABAergic neurons. Dysfunction of this GABA-generating enzyme is associated with epilepsy in mice (Kash et al., 1997). Although we could not find differences in GABA levels in hippocampus and parahippocampal cortex tissue by metabolomic analyses, proteomic findings pointed to alterations in GABA synthesis, release and degradation in hippocampal tissue. However, the fact that the GABA synthesizing enzyme GAD65 is upregulated in *Slc13a5*$^{-/-}$ mice indicates that these alterations may rather reflect compensatory changes. In this respect, it is interesting to note that patients with *SLC13A5* mutations exhibited some improvement in seizures by GABAergic antiepileptic drugs, including benzodiazepines and phenobarbital (Klotz et al., 2016).

Altered TCA cycle may also result in reduced ATP and adenosine levels, which would then result in reduced activation of adenosine A1 receptors with consequences of potassium channel regulation and resulting neuronal hyperexcitability (Shetty et al., 2012). This would contribute to the electrophysiological findings in *Slc13a5*$^{-/-}$ mice. It may also explain that the use of the ketogenic diet, a high-fat, low-carbohydrate diet was reported to be beneficial for seizure control or level of alertness and development in patients with *SLC13A5* mutations (Hardies et al., 2015), although also worsening of the disease has been reported (Klotz et al., 2016).

Further molecular alterations indicated by large-scale proteomic analysis may reflect either additional compensatory mechanisms or pathophysiological mechanisms contributing to seizure susceptibility. In the hippocampus of *Slc13a5*$^{-/-}$ mice, enzymes involved in degradation of monoamines including serotonin exhibited lowered expression levels. These proteome alterations may point to an activation of endogenous anticonvulsant mechanisms as a consequence of seizure activity. In this respect it is interesting to note that preclinical and clinical data on fenfluramine, which enhances release and inhibits reuptake of serotonin, suggest that increasing serotonin concentrations can prevent ictogenesis (Schoonjans and Ceulemans, 2019).

Extracellular matrix reorganization and dysregulation of lipid and lipoprotein metabolism are discussed as putative contributors to epileptogenesis and ictogenesis (Nistico and De Sarro, 1991; Pitkänen et al., 2014; Walker et al., 2016; Keck et al., 2018; Li et al., 2018). Thus, respective expression alterations identified in the parahippocampal cortex of *Slc13a5*$^{-/-}$ mice may contribute to enhanced excitability.

In theory, because SLC13A5 is also abundantly expressed in the liver, secondary contributing effects from altered liver metabolism might also play a role for the brain phenotype following SLC13A5 deletion as observed here. However, as previously reported by us for *Slc13a5*$^{-/-}$ mice, liver histology is normal in these mice, high fat diet fed *Slc13a5*$^{-/-}$ mice are protected from the non-alcoholic fatty liver disease that develops in the wild type mice, and *Slc13a5*$^{-/-}$ mice have increased levels of ketone bodies (due to an increase in hepatic lipid oxidation), which are in general regarded as protective against seizures (Birkenfeld et al., 2011). Thus, while we cannot completely exclude the possibility that peripheral metabolic changes contribute to the brain phenotype reported here, our previous data make it unlikely.

In summary, our data suggest that deletion of *Slc13a5* in mice contributes to an epileptic phenotype, reflecting the situation in the recently identified patients with loss-of-function *SLC13A5* mutations. The metabolomic data indicate that extracellular and intracellular citrate levels in the brain are involved in the observed epilepsy phenotype in mutant mice, substantiating the cytoplasmic citrate deficit hypothesis suggested by Bhutia et al. (2017), but also the zinc chelation and interneuron energy hypotheses suggested by the latter authors (Fig. 7). Since seizures and status epilepticus occurring in patients with *SLC13A5* mutations are typically resistant to available therapies (Klotz et al., 2016), the current mouse model provides a tool for further understanding the pathophysiology of seizures in response to *SLC13A5* mutations and developing novel, more effective therapies for this severe type of early infantile epileptic encephalopathy.

Supplementary data to this article can be found online at https://doi.org/10.1016/j.nbd.2020.105018.

Author contributions

A.L.B., W.L., J.J., H.P., R.K. and C.M.M. designed the study. C.H., K.T., R.M.v.D., N.M., T.C., F.T., S.B., V.Z., M.R., S.M.H., C.V., L.W., S.A.S., T.S., D.M.W., A.K., N.E., and S.R.B. performed the experiments and analyzed the data. W.L., C.H., H.P., R.K. and A.L.B. wrote the paper. All authors discussed the results and revised and approved the manuscript.

Credit author statement

A.L.B., W.L., J.J., H.P., R.K. and C.M.M. designed the study. C.H., K.T., R.M.v.D., N.M., T.C., F.T., S.B., V.Z., M.R., S.M.H., C.V., L.W., S.A.S., T.S., D.M.W., A.K., N.E., and S.R.B. performed the experiments and analyzed the data. W.L., C.H., H.P., R.K. and A.L.B. wrote the paper. All authors discussed the results and revised and approved the manuscript.

Acknowledgements

The authors thank Dr. Ingo Borggräfe (Pediatric Epileptology of the Epilepsy Center Munich, Germany), Dr. Lothar Kreienbrock (Institute for Biometry, Epidemiology, and Information Processing, University of Veterinary Medicine Hannover, Germany), and Dr. Brenda Porter (Department of Neurology, Stanford University School of Medicine, Palo Alto, California, U.S.) for discussions during preparation of the manuscript. This work was funded, in part, by support from the Tess Research Foundation (Menlo Park, CA, USA).

References

Alhakeem, A., Alshibani, F., Tabarki, B., 2018. Extending the use of stiripentol to SLC13A5-related epileptic encephalopathy. Brain Dev. 40, 827–829.
Amico-Ruvio, S.A., Murthy, S.E., Smith, T.P., Popescu, G.K., 2011. Zinc effects on NMDA receptor gating kinetics. Biophys. J. 100, 1910–1918.
Anderson, R.M., Weindruch, R., 2012. The caloric restriction paradigm: implications for healthy human aging. Am. J. Hum. Biol. 24, 101–106.
Anjum, S.M.M., Käufer, C., Hopfengärtner, R., Waltl, I., Bröer, S., Löscher, W., 2018. Automated quantification of EEG spikes and spike clusters as a new read out in Theiler's virus mouse model of encephalitis-induced epilepsy. Epilepsy Behav. 88, 189–204.
Bainbridge, M.N., Cooney, E., Miller, M., Kennedy, A.D., Wulff, J.E., Donti, T., Jhangiani, S.N., Gibbs, R.A., Elsea, S.H., Porter, B.E., Graham, B.H., 2017. Analyses of SLC13A5-epilepsy patients reveal perturbations of TCA cycle. Mol. Genet. Metab. 121, 314–319.
Barnard, G.A., 1947. Significance tests for 2 X 2 tables. Biometrika. 34, 123–138.
Behr, J., Heinemann, U., Mody, I., 2001. Kindling induces transient NMDA receptor-mediated facilitation of high-frequency input in the rat dentate gyrus. J. Neurophysiol. 85, 2195–2202.
Bergeron, M.J., Clemencon, B., Hediger, M.A., Markovich, D., 2013. SLC13 family of Na(+)-coupled di- and tri-carboxylate/sulfate transporters. Mol. Asp. Med. 34, 299–312.
Bhutia, Y.D., Kopel, J.J., Lawrence, J.J., Neugebauer, V., Ganapathy, V., 2017. Plasma membrane Na(+)-coupled citrate transporter (SLC13A5) and neonatal epileptic encephalopathy. Molecules. 22, 378.
Birkenfeld, A.L., Lee, H.Y., Guebre-Egziabher, F., Alves, T.C., Jurczak, M.J., Jornayvaz, F.R., Zhang, D., Hsiao, J.J., Martin-Montalvo, A., Fischer-Rosinsky, A., Spranger, J., Pfeiffer, A.F., Jordan, J., Fromm, M.F., Konig, J., Lieske, S., Carmean, C.M., Frederick, D.W., Weismann, D., Knauf, F., Irusta, P.M., De Cabo, R., Helfand, S.L., Samuel, V.T., Shulman, G.I., 2011. Deletion of the mammalian INDY homolog mimics aspects of dietary restriction and protects against adiposity and insulin resistance in mice. Cell Metab. 14, 184–195.
Bodnoff, S.R., Suranyi-Cadotte, B., Aitken, D.H., Quirion, R., Meaney, M.J., 1988. The effects of chronic antidepressant treatment in an animal model of anxiety. Psychopharmacology 95, 298–302.
Brehme, H., Kirschstein, T., Schulz, R., Köhling, R., 2014. In vivo treatment with the casein kinase 2 inhibitor 4,5,6,7- tetrabromotriazole augments the slow after-hyperpolarizing potential and prevents acute epileptiform activity. Epilepsia 55, 175–183.
Bröer, S., Kaufer, C., Haist, V., Li, L., Gerhauser, I., Anjum, M., Bankstahl, M., Baumgärtner, W., Löscher, W., 2016. Brain inflammation, neurodegeneration and seizure development following picornavirus infection markedly differ among virus and mouse strains and substrains. Exp. Neurol. 279, 57–74.
Cai, T., Parast, L., Ryan, L., 2010. Meta-analysis for rare events. Stat. Med. 29, 2078–2089.
Cesar, M., Hamprecht, B., 1995. Immunocytochemical examination of neural rat and mouse primary cultures using monoclonal antibodies raised against pyruvate carboxylase. J. Neurochem. 64, 2312–2318.
Cordes, T., Metallo, C.M., 2019. Quantifying intermediary metabolism and Lipogenesis in cultured mammalian cells using stable isotope tracing and mass spectrometry. Methods Mol. Biol. 1978, 219–241.
Coughenor, L.L., McLean, J.R., Parker, R.B., 1977. A new device for the rapid measurement of impaired motor function in mice. Pharmacol. Biochem. Behav. 6, 351–353.
Deng, W., Pleasure, J., Pleasure, D., 2008. Progress in periventricular leukomalacia. Arch. Neurol. 65, 1291–1295.
Dunham, N.W., Miya, T.S., 1957. A note on a simple apparatus for detecting neurological deficit in mice and rats. J. Am. Pharm. Assoc. 46, 208–209.
Field, T.B., Coburn, J., McCourt, J.L., McBryde, W.A.E., 1975. Composition and stability of some metal citrate and Diglycolate complexes in aqueous solution. Anal. Chim. Acta 74, 101–106.
Fisher, R.S., Scharfman, H.E., deCurtis, M., 2014. How can we identify ictal and interictal abnormal activity? Adv. Exp. Med. Biol. 813, 3–23.
Glusker, J.P., 1980. Conformation and chelation: enzymatic implications. Acc. Chem. Res. 13, 345–352.
Grinspan, Z.M., Tian, N., Yozawitz, E.G., McGoldrick, P.E., Wolf, S.M., McDonough, T.L., Nelson, A., Hafeez, B., Johnson, S.B., Hesdorffer, D.C., 2018. Common terms for rare epilepsies: synonyms, associated terms, and links to structured vocabularies. Epilepsia Open 3, 91–97.
Hardies, K., de Kovel, C.G., Weckhuysen, S., Asselbergh, B., Geuens, T., Deconinck, T., Azmi, A., May, P., Brilstra, E., Becker, F., Barisic, N., Craiu, D., Braun, K.P., Lal, D., Thiele, H., Schubert, J., Weber, Y., van 't, S.R., Nurnberg, P., Balling, R., Timmerman, V., Lerche, H., Maudsley, S., Helbig, I., Suls, A., Koeleman, B.P., De Jonghe, P., 2015. Recessive mutations in SLC13A5 result in a loss of citrate transport and cause neonatal epilepsy, developmental delay and teeth hypoplasia. Brain 138, 3238–3250.
Hassel, B., 2001. Pyruvate carboxylation in neurons. J. Neurosci. Res. 66, 755–762.
Hassel, B., Brathe, A., 2000. Neuronal pyruvate carboxylation supports formation of transmitter glutamate. J. Neurosci. 20, 1342–1347.
Hornfeldt, C.S., Larson, A.A., 1990. Seizures induced by fluoroacetic acid and fluorocitric acid may involve chelation of divalent cations in the spinal cord. Eur. J. Pharmacol. 179, 307–313.
Huard, K., Gosset, J.R., Montgomery, J.I., Gilbert, A., Hayward, M.M., Magee, T.V., Cabral, S., Uccello, D.P., Bahnck, K., Brown, J., Purkal, J., Gorgoglione, M., Lanba, A., Futatsugi, K., Herr, M., Genung, N.E., Aspnes, G., Polivkova, J., Garcia-Irizarry, C.N., Li, Q., Canterbury, D., Niosi, M., Vera, N.B., Li, Z., Khunte, B., Siderewicz, J., Rolph, T., Erion, D.M., 2016. Optimization of a Dicarboxylic series for in vivo inhibition of citrate transport by the solute carrier 13 (SLC13) family. J. Med. Chem. 59, 1165–1175.
Iacobazzi, V., Infantino, V., 2014. Citrate–new functions for an old metabolite. Biol. Chem. 395, 387–399.
Inoue, K., Zhuang, L., Maddox, D.M., Smith, S.B., Ganapathy, V., 2002a. Structure, function, and expression pattern of a novel sodium-coupled citrate transporter (NaCT) cloned from mammalian brain. J. Biol. Chem. 277, 39469–39476.
Inoue, K., Zhuang, L., Ganapathy, V., 2002b. Human Na+ −coupled citrate transporter: primary structure, genomic organization, and transport function. Biochem. Biophys. Res. Commun. 299, 465–471.
Irwin, S., 1968. Comprehensive observational assessment: Ia. A systematic, quantitative procedure for assessing the behavioral and physiologic state of the mouse. Psychopharmacologia. 13, 222–257.
Italiano, D., Striano, P., Russo, E., Leo, A., Spina, E., Zara, F., Striano, S., Gambardella, A., Labate, A., Gasparini, S., Lamberti, M., De Sarro, G., Aguglia, U., Ferlazzo, E., 2016. Genetics of reflex seizures and epilepsies in humans and animals. Epilepsy Res. 121, 47–54.
Johnson, N.L., Kemp, A.W., and Kotz, S. (2005). Univariate Discrete Distributions, 3rd Edition. (New York: Wiley).
Kalappa, B.I., Tzounopoulos, T., 2017. Context-dependent modulation of excitatory synaptic strength by Synaptically released zinc. eNeuro. 4, e0011-e0017.
Kamburov, A., Wierling, C., Lehrach, H., Herwig, R., 2009. ConsensusPathDB–a database for integrating human functional interaction networks. Nucleic Acids Res. 37, D623–D628.
Kann, O., 2016. The interneuron energy hypothesis: implications for brain disease. Neurobiol. Dis. 90, 75–85.
Kash, S.F., Johnson, R.S., Tecott, L.H., Noebels, J.L., Mayfield, R.D., Hanahan, D., Baekkeskov, S., 1997. Epilepsy in mice deficient in the 65-kDa isoform of glutamic acid decarboxylase. Proc. Natl. Acad. Sci. U. S. A. 94, 14060–14065.
Keck, M., van Dijk, R.M., Deeg, C.A., Kistler, K., Walker, A., von Ruden, E.L., Russmann, V., Hauck, S.M., Potschka, H., 2018. Proteomic profiling of epileptogenesis in a rat model: focus on cell stress, extracellular matrix and angiogenesis. Neurobiol. Dis. 112, 119–135.
Kilkenny, C., Browne, W.J., Cuthill, I.C., Emerson, M., Altman, D.G., 2010. Improving bioscience research reporting: the ARRIVE guidelines for reporting animal research. PLoS Biol. 8, e1000412.
Klee, R., Töllner, K., Rankovic, V., Römermann, K., Schidlitzki, A., Bankstahl, M., Löscher, W., 2015. Network pharmacology for antiepileptogenesis: tolerability of multi-targeted drug combinations in nonepileptic vs. post-status epilepticus mice. Epilepsy Res. 118, 34–48.
Klotz, J., Porter, B.E., Colas, C., Schlessinger, A., Pajor, A.M., 2016. Mutations in the Na(+)/citrate cotransporter NaCT (SLC13A5) in pediatric patients with epilepsy and developmental delay. Mol. Med. 22, 310–321.
Kurtz, B.S., Lehman, J., Garlick, P., Amberg, J., Mishra, P.K., Dailey, J.W., Weber, R., Jobe, P.C., 2001. Penetrance and expressivity of genes involved in the development of epilepsy in the genetically epilepsy-prone rat (GEPR). J. Neurogenet. 15, 233–244.
Lamp, J., Keyser, B., Koeller, D.M., Ullrich, K., Braulke, T., Muhlhausen, C., 2011. Glutaric

aciduria type 1 metabolites impair the succinate transport from astrocytic to neuronal cells. J. Biol. Chem. 286, 17777–17784.
Lepper, M.F., Ohmayer, U., von Toerne, C., Maison, N., Ziegler, A.G., Hauck, S.M., 2018. Proteomic landscape of patient-derived CD4+ T cells in recent-onset type 1 diabetes. J. Proteome Res. 17, 618–634.
Li, S., Kumar, T.P., Joshee, S., Kirschstein, T., Subburaju, S., Khalili, J.S., Kloepper, J., Du, C., Elkhal, A., Szabo, G., Jain, R.K., Köhling, R., Vasudevan, A., 2018. Endothelial cell-derived GABA signaling modulates neuronal migration and postnatal behavior. Cell Res. 28, 221–248.
Liu, A., Yang, X., Yang, X., Wu, Q., Zhang, J., Sun, D., Yang, Z., Jiang, Y., Wu, X., Wei, L., Zhang, Y., 2019. Mosaicism and incomplete penetrance of PCDH19 mutations. J. Med. Genet. 56, 81–88.
Liu, L., Duff, K., 2008. A technique for serial collection of cerebrospinal fluid from the cisterna magna in mouse. J. Vis. Exp. (21), 260.
von Loeffelholz, C., Lieske, S., Neuschafer-Rube, F., Willmes, D.M., Raschzok, N., Sauer, I.M., Konig, J., Fromm, M.F., Horn, P., Chatzigeorgiou, A., Pathe-Neuschafer-Rube, A., Jordan, J., Pfeiffer, A.F.H., Mingrone, G., Bornstein, S.R., Stroehle, P., Harms, C., Wunderlich, F.T., Helfand, S.L., Bernier, M., De Cabo, R., Shulman, G.I., Chavakis, T., Puschel, G.P., Birkenfeld, A.L., 2017. The human longevity gene homolog INDY and interleukin-6 interact in hepatic lipid metabolism. Hepatology 66, 616–630.
Löscher, W., 2017. Animal models of seizures and epilepsy: past, present, and future role for the discovery of Antiseizure drugs. Neurochem. Res. 42, 1873–1888.
Löscher, W., Ebert, U., 1996. The role of the piriform cortex in kindling. Prog. Neurobiol. 50, 427–481.
Lydersen, S., Fagerland, M.W., Laake, P., 2009. Recommended tests for association in 2 x 2 tables. Stat. Med. 28, 1159–1175.
Magistretti, P.J., Allaman, I., 2015. A cellular perspective on brain energy metabolism and functional imaging. Neuron 86, 883–901.
McDougal Jr., D.B., Cowsette, B.R., Pusateri, M.E., Carter, J.G., Manchester, J.K., Chi, M.M., Lowry, O.H., 1997. Glutamate and potassium stimulation of hippocampal slices metabolizing glucose or glucose and pyruvate. Brain Res. 755, 304–312.
McIntyre, D.C., Gilby, K.L., 2008. Mapping seizure pathways in the temporal lobe. Epilepsia 49 (Suppl. 3), 23–30.
Molin, S., Merl, J., Dietrich, K.A., Regauer, M., Flaig, M., Letule, V., Saucke, T., Herzinger, T., Ruzicka, T., Hauck, S.M., 2015. The hand eczema proteome: imbalance of epidermal barrier proteins. Br. J. Dermatol. 172, 994–1001.
Morris, R., 1984. Developments of a water-maze procedure for studying spatial learning in the rat. J. Neurosci. Methods 11, 47–60.
Müller, C.J., Gröticke, I., Bankstahl, M., Löscher, W., 2009. Behavioral and cognitive alterations, spontaneous seizures, and neuropathology developing after a pilocarpine-induced status epilepticus in C57BL/6 **mice**. Exp Neurol. 219, 284–297.
Müller, L., Tokay, T., Porath, K., Köhling, R., Kirschstein, T., 2013. Enhanced NMDA receptor-dependent LTP in the epileptic CA1 area via upregulation of NR2B. Neurobiol. Dis. 54, 183–193.
Mulley, J.C., Mefford, H.C., 2011. Epilepsy and the new cytogenetics. Epilepsia 52, 423–432.
Nadel, L., 2000. The parahippocampal region: basic science and clinical implications. Hippocampus 10, 133–135.
Nistico, G., De Sarro, G., 1991. Behavioral and electrocortical spectrum power effects after microinfusion of lymphokines in several areas of the rat brain. Ann. N. Y. Acad. Sci. 621, 119–134.
Pajor, A.M., 2014. Sodium-coupled dicarboxylate and citrate transporters from the SLC13 family. Pflugers Arch. 466, 119–130.
Pajor, A.M., Gangula, R., Yao, X., 2001. Cloning and functional characterization of a high-affinity Na(+)/dicarboxylate cotransporter from mouse brain. Am. J. Phys. Cell Phys. 280, C1215–C1223.
Paoletti, P., Ascher, P., Neyton, J., 1997. High-affinity zinc inhibition of NMDA NR1-NR2A receptors. J. Neurosci. 17, 5711–5725.
Paxinos, G., Franklin, K.B.J. (2001). The Mouse Brain in Stereotaxic Coordinates., G. Paxinos and K.B.J. Franklin, eds. (New York: Academic Press).
Pesta, D.H., Perry, R.J., Guebre-Egziabher, F., Zhang, D., Jurczak, M., Fischer-Rosinsky, A., Daniels, M.A., Willmes, D.M., Bhanot, S., Bornstein, S.R., Knauf, F., Samuel, V.T., Shulman, G.I., Birkenfeld, A.L., 2015. Prevention of diet-induced hepatic steatosis and hepatic insulin resistance by second generation antisense oligonucleotides targeted to the longevity gene mIndy (Slc13a5). Aging (Albany NY) 7, 1086–1093.
Pitkänen, A., Ndode-Ekane, X.E., Lukasiuk, K., Wilczynski, G.M., Dityatev, A., Walker, M.C., Chabrol, E., Dedeurwaerdere, S., Vazquez, N., Powell, E.M., 2014. Neural ECM and epilepsy. Prog. Brain Res. 214, 229–262.
R Core Team (2013). A Language and Environment for Statistical Computing. http://www. R-project. org/.
Racine, R.J., 1972. Modification of seizure activity by electrical stimulation: II. Motor seizure. Electroencephalogr. Clin. Neurophysiol. 32, 281–294.
Riban, V., Bouilleret, V., Pham, L., Fritschy, J.M., Marescaux, C., Depaulis, A., 2002. Evolution of hippocampal epileptic activity during the development of hippocampal sclerosis in a mouse model of temporal lobe epilepsy. Neuroscience 112, 101–111.
Rogina, B., Reenan, R.A., Nilsen, S.P., Helfand, S.L., 2000. Extended life-span conferred by cotransporter gene mutations in Drosophila. Science 290, 2137–2140.
Romero-Hernandez, A., Simorowski, N., Karakas, E., Furukawa, H., 2016. Molecular basis for subtype specificity and high-affinity zinc inhibition in the GluN1-GluN2A NMDA receptor amino-terminal domain. Neuron 92, 1324–1336.
Ros, S., Schulze, A., 2013. Balancing glycolytic flux: the role of 6-phosphofructo-2-kinase/fructose 2,6-bisphosphatases in cancer metabolism. Cancer Metab 1, 8.
Sato, O., Yamguchi, T., Kittaka, M., Toyama, H., 2001. Hydrocephalus and epilepsy. Childs Nerv. Syst. 17, 76–86.
Scharfman, H.E., 2000. Epileptogenesis in the parahippocampal region. Parallels with the dentate gyrus. Ann. N. Y. Acad. Sci. 911, 305–327.
Schoonjans, A.S., Ceulemans, B., 2019. An old drug for a new indication: repurposing Fenfluramine from an Anorexigen to an antiepileptic drug. Clin. Pharmacol. Ther. 106, 929–932.
Schossig, A., Bloch-Zupan, A., Lussi, A., Wolf, N.I., Raskin, S., Cohen, M., Giuliano, F., Jurgens, J., Krabichler, B., Koolen, D.A., Macena Sobreira, N.L., Maurer, E., Muller-Bolla, M., Penzien, J., Zschocke, J., Kapferer-Seebacher, I., 2017. SLC13A5 is the second gene associated with Kohlschutter-Tonz syndrome. J. Med. Genet. 54, 54–62.
Selch, S., Chafai, A., Sticht, H., Birkenfeld, A.L., Fromm, M.F., Konig, J., 2018. Analysis of naturally occurring mutations in the human uptake transporter NaCT important for bone and brain development and energy metabolism. Sci. Rep. 8, 11330.
Shank, R.P., Bennett, G.S., Freytag, S.O., Campbell, G.L., 1985. Pyruvate carboxylase: an astrocyte-specific enzyme implicated in the replenishment of amino acid neurotransmitter pools. Brain Res. 329, 364–367.
Shephard, R.A., Broadhurst, P.L., 1982. Effects of diazepam and picrotoxin on hyponeophagia in rats. Neuropharmacology 21, 771–773.
Shetty, P.K., Galeffi, F., Turner, D.A., 2012. Cellular links between neuronal activity and energy homeostasis. Front. Pharmacol. 3, 43.
Smith, B.N., Dudek, F.E., 2001. Short- and long-term changes in CA1 network excitability after kainate treatment in rats. J. Neurophysiol. 85, 1–9.
Sonnewald, U., Westergaard, N., Krane, J., Unsgard, G., Petersen, S.B., Schousboe, A., 1991. First direct demonstration of preferential release of citrate from astrocytes using [13C]NMR spectroscopy of cultured neurons and astrocytes. Neurosci. Lett. 128, 235–239.
Thevenon, J., Milh, M., Feillet, F., St Onge, J., Duffourd, Y., Juge, C., Roubertie, A., Heron, D., Mignot, C., Raffo, E., Isidor, B., Wahlen, S., Sanlaville, D., Villeneuve, N., Darmency-Stamboul, V., Toutain, A., Lefebvre, M., Chouchane, M., Huet, F., Lafon, A., de Saint, M.A., Lesca, G., El Chehadeh, S., Thauvin-Robinet, C., Masurel-Paulet, A., Odent, S., Villard, L., Philippe, C., Faivre, L., Riviere, J.B., 2014. Mutations in SLC13A5 cause autosomal-recessive epileptic encephalopathy with seizure onset in the first days of life. Am. J. Hum. Genet. 95, 113–120.
Töllner, K., Twele, F., Löscher, W., 2016. Evaluation of the pentylenetetrazole seizure threshold test in epileptic mice as surrogate model for drug testing against pharmacoresistant seizures. Epilepsy Behav. 57, 95–104.
Twele, F., Schidlitzki, A., Töllner, K., Löscher, W., 2017. The intrahippocampal kainate mouse model of mesial temporal lobe epilepsy: lack of electrographic seizure-like events in sham controls. Epilepsia Open 2, 180–187.
Vogel, P., Read, R.W., Hansen, G.M., Payne, B.J., Small, D., Sands, A.T., Zambrowicz, B.P., 2012. Congenital hydrocephalus in genetically engineered mice. Vet. Pathol. 49, 166–181.
Wada, M., Shimada, A., Fujita, T., 2006. Functional characterization of Na+ −coupled citrate transporter NaC2/NaCT expressed in primary cultures of neurons from mouse cerebral cortex. Brain Res. 1081, 92–100.
Walker, A., Russmann, V., Deeg, C.A., von Toerne, C., Kleinwort, K.J.H., Szober, C., Rettenbeck, M.L., von Ruden, E.L., Goc, J., Ongerth, T., Boes, K., Salvamoser, J.D., Vezzani, A., Hauck, S.M., Potschka, H., 2016. Proteomic profiling of epileptogenesis in a rat model: focus on inflammation. Brain Behav. Immun. 53, 138–158.
Warnes, G.R., Bolker, B., Bonebakker, L., Gentleman, R., Huber, W., Liaw, W., Lumley, T., Maechler, M., Magnusson, A., Moeller, S., 2015. Gplots: Various R Programming Tools for Plotting Data. R Package Version 2. 17. 0.
Weeke, L.C., Brilstra, E., Braun, K.P., Zonneveld-Huijssoon, E., Salomons, G.S., Koeleman, B.P., van Gassen, K.L., van Straaten, H.L., Craiu, D., De Vries, L.S., 2017. Punctate white matter lesions in full-term infants with neonatal seizures associated with SLC13A5 mutations. Eur. J. Paediatr. Neurol. 21, 396–403.
Westergaard, N., Banke, T., Wahl, P., Sonnewald, U., Schousboe, A., 1995. Citrate modulates the regulation by Zn2+ of N-methyl-D-aspartate receptor-mediated channel current and neurotransmitter release. Proc. Natl. Acad. Sci. U. S. A. 92, 3367–3370.
Westergaard, N., Waagepetersen, H.S., Belhage, B., Schousboe, A., 2017. Citrate, a ubiquitous key metabolite with regulatory function in the CNS. Neurochem. Res. 42, 1583–1588.
Wilkins, M.E., Smart, T.G., 2002. Redox modulation of GABAA receptors obscured by Zn2+ complexation. Neuropharmacology 43, 938–944.
Willmes, D.M., Birkenfeld, A.L., 2013. The role of INDY in metabolic regulation. Comput. Struct. Biotechnol. J. 6, e201303020.
Willmes, D.M., Kurzbach, A., Henke, C., Schumann, T., Zahn, G., Heifetz, A., Jordan, J., Helfand, S.L., Birkenfeld, A.L., 2018. The longevity gene INDY (I'm not dead yet) in metabolic control: potential as pharmacological target. Pharmacol. Ther. 185, 1–11.
Wozny, C., Gabriel, S., Jandova, K., Schulze, K., Heinemann, U., Behr, J., 2005. Entorhinal cortex entrains epileptiform activity in CA1 in pilocarpine-treated rats. Neurobiol. Dis. 19, 451–460.
Yodoya, E., Wada, M., Shimada, A., Katsukawa, H., Okada, N., Yamamoto, A., Ganapathy, V., Fujita, T., 2006. Functional and molecular identification of sodium-coupled dicarboxylate transporters in rat primary cultured cerebrocortical astrocytes and neurons. J. Neurochem. 97, 162–173.
Yu, A.C., Drejer, J., Hertz, L., Schousboe, A., 1983. Pyruvate carboxylase activity in primary cultures of astrocytes and neurons. J. Neurochem. 41, 1484–1487.